Dysfunction of specific auditory fibers impacts cortical oscillations, driving an autism phenotype despite near-normal hearing

Philine Marchetta, Konrad Dapper, Morgan Hess, Dila Calis, Wibke Singer, Jakob Wertz, Stefan Fink, Steffen Hage, Mesbah Alam, Kerstin Schwabe, et al.

Received: 29 September 2023 | Revised: 4 December 2023 | Accepted: 22 December 2023

DOI: 10.1096/fj.202301995R

RESEARCH ARTICLE

The FASEB Journal

Dysfunction of specific auditory fibers impacts cortical oscillations, driving an autism phenotype despite near-normal hearing

Philine Marchetta[1] | **Konrad Dapper**[1] | **Morgan Hess**[1] | **Dila Calis**[1] | **Wibke Singer**[1] | **Jakob Wertz**[1] | **Stefan Fink**[1] | **Steffen R. Hage**[2] | **Mesbah Alam**[3] | **Kerstin Schwabe**[3] | **Robert Lukowski**[4] | **Jerome Bourien**[5] | **Jean-Luc Puel**[5] | **Michele H. Jacob**[6] | **Matthias H. J. Munk**[7,8] | **Rüdiger Land**[9] | **Lukas Rüttiger**[1] | **Marlies Knipper**[1]

[1]Molecular Physiology of Hearing, Department of Otolaryngology, Head and Neck Surgery, Tübingen Hearing Research Centre, University of Tübingen, Tübingen, Germany

[2]Werner Reichardt Centre for Integrative Neuroscience, University of Tübingen, Tübingen, Germany

[3]Experimental Neurosurgery, Department of Neurosurgery, Hannover Medical School, Hannover, Germany

[4]Institute of Pharmacy, Pharmacology, Toxicology and Clinical Pharmacy, University of Tübingen, Tübingen, Germany

[5]Institute for Neurosciences Montpellier, Institut National de la Santé et de la Recherche Médical, University of Montpellier, Montpellier, France

[6]Department of Neuroscience, Tufts University School of Medicine, Sackler School of Biomedical Sciences, Boston, Massachusetts, USA

[7]Department of Psychiatry & Psychotherapy, University of Tübingen, Tübingen, Germany

[8]Department of Biology, Technical University Darmstadt, Darmstadt, Germany

[9]Department of Experimental Otology, Institute of Audioneurotechnology, Hannover Medical School, Hannover, Germany

Correspondence
Marlies Knipper, Molecular Physiology of Hearing, University ENT Clinic Tübingen, Elfriede-Aulhorn-Str.5, 72076 Tübingen, Germany.
Email: marlies.knipper@uni-tuebingen.de

Funding information
Deutsche Forschungsgemeinschaft (DFG), Grant/Award Number: RU 713/3-2, KN 316/12-1, GRK

Abstract

Autism spectrum disorder is discussed in the context of altered neural oscillations and imbalanced cortical excitation–inhibition of cortical origin. We studied here whether developmental changes in peripheral auditory processing, while preserving basic hearing function, lead to altered cortical oscillations. Local field potentials (LFPs) were recorded from auditory, visual, and prefrontal cortices and the hippocampus of *Bdnf*^{Pax2} KO mice. These mice develop an autism-like behavioral phenotype through deletion of BDNF in Pax2+ interneuron

Abbreviations: AC, auditory cortex; ANF, auditory nerve fiber; Arc, activity-regulated cytoskeletal protein; ASSRs, amplitude-modulated auditory steady-state responses; BDNF, brain derived neurotrophic factor; CAP, compound action potential; dB, decibel; DC, direct current; DCN, dorsal cochlear nucleus; E/I, excitatory vs inhibitory; EEG, electroencephalographic; ERP, event related potentials; FFT, fast Fourier transformation; GABA, gamma-aminobutyric acid; HC, hippocampus; IC, inferior colliculus; IN, interneuron; I/O, input-output; ISI, inter stimulus interval; KCC2, potassium chloride cotransporter 2; kHz, kilo Hertz; KO, knock out; LFP, local field potential; LOC, lateral olivocochlear; LWR, length to width ratio; MGB, medial geniculate body; PFC, prefrontal cortex; PSTRs, peristimulus time responses; PV, parvalbumin; ROI, region of interest; SEM, standard error of the mean; SPL, sound pressure level; SR, spontaneous firing rate; V1, visual cortex; vGlut1, vesicular glutamate transporter 1.

Philine Marchetta, Konrad Dapper, and Morgan Hess contributed equally to the manuscript.

2381 and Cluster of Excellence 2177 "Hearing4all" Project number 390895286; ERA-NET NEURON JTC 2020, Grant/Award Number: BMBF 01EW2102 CoSySpeech FWO G0H6420N

precursors, affecting lower brainstem functions, but not frontal brain regions directly. Evoked LFP responses to behaviorally relevant auditory stimuli were weaker in the auditory cortex of *Bdnf*^{Pax2} KOs, connected to maturation deficits of high-spontaneous rate auditory nerve fibers. This was correlated with enhanced spontaneous and induced LFP power, excitation–inhibition imbalance, and dendritic spine immaturity, mirroring autistic phenotypes. Thus, impairments in peripheral high-spontaneous rate fibers alter spike synchrony and subsequently cortical processing relevant for normal communication and behavior.

KEYWORDS

auditory nerve fibers, autism spectrum disorder, BDNF, cortical oscillations, fast auditory processing, GABAergic interneurons, parvalbumin

1 | INTRODUCTION

Autism describes a constellation of early-appearing social communication deficits.[1] Though it is thought to have a genetic basis, with Fragile X Syndrome being the leading inherited cause, a majority of cases are idiopathic.[2] There is mounting evidence that autism originates from disruptions of intracortical circuits during a critical developmental period of multiple sensory systems.[3–5] This becomes evident through reduced frontal electroencephalographic (EEG) power across all brain oscillation frequencies, a characteristic neural marker in autistic infants.[6,7]

The generation of neural oscillations depends on the proper maturation of inhibitory interneurons, specifically fast-spiking, parvalbumin (PV)-expressing cells.[8–11] Therefore, the pathological features of autism are generally discussed in the context of reduced cortical stimulus-driven PV-interneuron (IN) function.[3,5,12] Altered brain oscillations have been observed in numerous developmental disorders that are characterized by an imbalance of excitatory versus inhibitory (E/I) activity, the origin of which remains unclear.[5,13–15] Some studies discuss E/I imbalance in neuropsychiatric disorders, including autism, in the context of impairments of PV-IN progenitors migrating to the telencephalon.[16] Others suggest autism to be a "critical period" disorder characterized by a disturbed temporal integration of sensory inputs within and across sensory modalities, important for a coherent representation of information.[3–5,14,17,18] As cortical PV cells determine the sequential nature of critical periods and related maturation of sensory modalities,[5,19] both theories focus on dysfunctional PV cells in the cortex as a causal factor of autism.

We previously described[20] an autistic-like phenotype in mice in which brain derived neurotrophic factor (BDNF) was deleted in Pax2-lineage descendants in hindbrain regions (*Bdnf*^{Pax2} KO). This phenotype included deficits in learning, social behavior, and anxiety.[20] The deletion, however, left numbers of cortical and hippocampal PV-INs and BDNF levels in frontal brain regions unaffected.[20,21] As BDNF drives synaptogenesis of the cortical PV-IN network,[22,23] normal BDNF levels in frontal brain regions of *Bdnf*^{Pax2} KO mice exclude a contribution of cortical BDNF to the autism phenotype. *Bdnf*^{Pax2} KO mice also exhibited normal basic hearing thresholds, but lower amplitude and delayed supra-threshold auditory nerve responses, linked to a reduced dynamic range, elevated spontaneous firing rates (SRs), delayed first-spike latency, and impaired inhibitory strength of high-frequency sidebands in neurons of the dorsal cochlear nucleus (DCN)[20] and the inferior colliculus (IC).[21] In addition, despite normal numbers of PV-INs, *Bdnf*^{Pax2} KO mice showed reduced dendritic PV staining in the auditory cortex (AC) and hippocampus (HC), which correlated with deficits in learning and social behavior and with increased anxiety, altogether displaying an autistic-like phenotype.[20]

Subpallium-derived GABAergic IN precursors, which have been discussed in the context of autism,[16,24,25] are positive for the transcription factor Pax6[26] and migrate to the telencephalon. In contrast, Pax2+ IN precursors migrate from the ventricular zones to lower, more posterior brain levels, such as the cerebellum, hindbrain, and spinal cord.[27–29] This might suggest deficits relating to the autistic phenotype in *Bdnf*^{Pax2} KO mice may originate in the brainstem rather than in the frontal cortical brain regions.

Thus, our overarching goal was to determine whether the autistic phenotype observed in *Bdnf*^{Pax2} KO mice could be caused primarily by a peripheral deficit in the lower auditory brainstem regions. We investigated this by addressing the following points:

(i) The first aim was to examine whether *Bdnf*^{Pax2} KO mice display typical changes of brain oscillations or other signs of E/I imbalance that are commonly seen in autism spectrum disorders.[6,7]

(ii) The second aim was to explore whether the source of these cortical changes in *Bdnf*^{Pax2} KO mice can be attributed to a peripheral origin. We aimed to identify the source of altered cortical brain activity in the periphery of *Bdnf*^{Pax2} KO mice with normal basic hearing function.

Addressing (i), we analyzed cortical local field potentials (LFPs) in the AC, prefrontal cortex (PFC), visual cortex (V1), and HC in response to auditory stimuli of behaviorally relevant frequencies and intensity levels, amplitude-modulated auditory steady-state responses (ASSRs), and stimulus-evoked (phase-coherent), induced (phase-incoherent), and spontaneous (resting-state) brain oscillations.[30] As we present auditory stimuli, V1 was used as a control region which should not directly respond to sound stimuli but may still be affected by intracortical feedback. Additionally, markers of E/I imbalance, such as vesicular glutamate transporter 1 (vGlut1) and PV, were analyzed in addition to spine morphology upon Golgi's staining.

Addressing (ii), we analyzed compound action potential (CAP) thresholds and peristimulus time responses (PSTRs) in the same frequency ranges presented during LFP recordings. Both approaches provide information about the spike synchronization within auditory fibers and might identify relations between peripheral and cortical responses.

A connection was observed between deficits in synchronized response behavior of high-SR auditory nerve fiber (ANF) processing and reduced evoked and enhanced induced EEG power in *Bdnf*^{Pax2} KO mice.

2 | MATERIALS AND METHODS

2.1 | Animals

The care and use of mice and the experimental protocol were reviewed and approved by the University of Tübingen, Veterinary Care Unit, and by the Animal Care and Ethics Committee of the Regional Board of the Federal State Government of Baden-Württemberg, Germany, and followed the guidelines of the European Union Directive 2010/63/EU for animal experiments. *Bdnf*^{Pax2} KO and control mice were obtained by crossing the Pax2^{Cre} mouse line[31] with the *Bdnf*^{flox} mouse line.[32] Both lines were obtained from the Mutant Mouse Regional Research Center, MMRRC.[33] For all experiments, adult mice between ten weeks and six months old of either sex were used.

2.2 | Tissue preparation

Tissue preparation was carried out as previously described in detail.[34] In brief, brains were dissected and fixed in 2% paraformaldehyde for 48 h and then stored in 1% paraformaldehyde at 4°C until sectioned. Brains were sectioned at 40–60 µm on a VT1000S Leica vibratome (Leica, Wetzlar, Germany). Sections were stored at −20°C in cryoprotectant (150 g of sucrose in 200 mL 1× PBS and 150 mL ethylene glycol, volume adjusted to 500 mL with 1× PBS) until use.

2.3 | Immunohistochemistry

Immunohistochemistry was carried out as described in detail previously.[35] Sections were selected according to the mouse brain atlas[36] focusing on hippocampal regions between −1.7 and −2.45 bregma. In brief, slices were washed in PBS (pH 7.2) followed by a permeabilization and blocking step using 3% BSA in PBS containing 0.2% Triton-X 100. Primary antibodies against PV (rabbit, diluted 1:2000, Abcam, Cambridge, UK) and vGlut1 (guinea pig, diluted 1:1000, Synaptic Systems, Göttingen, Germany) were diluted in 1.5% BSA in PBS containing 0.1% Triton-X 100. Slices were incubated with primary antibodies overnight at 4°C. After removing the antibody solution, slices were washed in PBS and primary antibodies were detected using secondary antibodies Cy3 (anti-rabbit, 1:1500, Jackson ImmunoResearch Laboratories, West Grove, PA, USA) and Alexa 488 (anti-guinea pig, 1:500, Molecular Probes, Eugene, OR, USA) diluted in 1.5% BSA in PBS containing 0.1% Triton-X 100. After 1h incubation with secondary antibodies at room temperature, slices were washed again in PBS and finally embedded using Vectashield mounting medium with DAPI.

Stained samples of 10 control mice and 12 *Bdnf*^{Pax2} KO mice were viewed using an upgraded Olympus BX61 microscope (EVIDENT Europe GmbH, Hamburg, Germany). Images were acquired using a Hamamatsu ORCA-Flash4.0 LT PLUS monochrome camera (Hamamatsu Photonics K.K., Herrsching, Germany) and analyzed with cellSens Dimension software (OSIS GmbH, Münster, Germany). To increase spatial resolution, slices were imaged over a distance of ∼15 µm within an image stack along the *z*-axis (*z*-stack), followed by 3-dimensional deconvolution using cellSens Dimension's built-in algorithm.

2.4 | Toluidine blue staining

Electrode position was confirmed using toluidine blue staining, using 1% toluidine blue in acetate buffer (pH 3.9). Slices were washed for five minutes with PBS and then submerged in the toluidine blue solution for 30 seconds before being washed two times with double-distilled water.

2.5 | Co-localization of mRNA and protein in brain sections

Sections were selected according to the mouse brain atlas[36] between −1.7 and −2.45 bregma. mRNA and protein were co-localized on free-floating brain sections as previously described[37] to enable the direct correlation of changes in expression patterns of excitatory and inhibitory markers that are mainly visible on either mRNA (activity-regulated cytoskeletal protein (Arc)/BDNF) or protein (PV) level. Sections were incubated overnight with BDNF or Arc riboprobes as previously described.[20] For protein detection, sections were incubated overnight at 4°C with a primary antibody against PV (anti-rabbit, 1:500, ab11427, Abcam, United Kingdom), followed by incubation with the secondary antibody (biotinylated goat anti-rabbit, BA-1000, Vector Laboratories).

All samples were viewed using the upgraded Olympus BX61 microscope (EVIDENT Europe GmbH, Hamburg, Germany). Images were acquired using a DP 71 bright-field camera (EVIDENT Europe GmbH).

2.6 | Anesthesia

Animals were anesthetized with intraperitoneal injections of fentanyl (0.05 mg/kg body weight, Fentanyl-hameln, Hameln Pharma plus GmbH, Hameln, Germany), midazolam (2.5 mg/kg body weight, Midazolam-hameln, Hameln Pharma plus GmbH), medetomidine (0.5 mg/kg body weight, Sedator, Albrecht GmbH, Aulendorf, Germany), and atropine sulfate (0.2 mg/kg body weight, B. Braun, Melsungen, Germany). Additional doses of anesthetics were administered if needed.

2.7 | Electrocochleographic recordings

Electrical potentials of ANFs were examined in anesthetized nine control mice and ten *Bdnf*^{Pax2} KO mice by electrocochleography. The mice were anesthetized as described above, and then, 20–40 µL Xylocaine 2% (AstraZeneca, Wedel, Germany) was applied subcutaneously at sites of surgical incisions. Mice were laid on a pre-warmed resting pad (37°C). The bony auditory bulla was exposed by cutting the skin behind the ear and carefully moving muscles, nerves, and connective tissues aside. A small hole (0.6 mm diameter) was drilled into the bulla in order to access the round-window niche of the cochlea. A silver wire electrode insulated with varnish and silicone that had a small silver bead at the tip was placed within the niche. The skin above the ear was closed, and the mouse was placed in the sound-attenuating booth in front of a loudspeaker for recording. CAP threshold responses from the auditory nerves were measured by stimulation with short tone pips (3ms duration including 1ms on- and off-ramp cos^2-shaped, 32–96 repetitions with stimulus interval 16 ms and alternating polarity) presented with 5 dB 12 incremental steps from 0 to 100 between 2 and 34 kHz. Electrical potentials were amplified (80 dB) and filtered between 0.2 and 5 kHz before being sampled at 20 kHz A/D rate, averaged, and saved to file. Thresholds were determined from individual ears from averaged waveform responses as the lowest sound pressure level (SPL), resulting in a signal visually distinguishable from noise.

For the CAP latency, electrical responses were recorded for 100 µs click stimuli of 0 to 100 dB SPL. Responses were amplified, filtered (DC, 50 kHz low pass), sampled at 100 kHz A/D rate, and averaged for 64 repetitions (interstimulus interval (ISI) 50 ms). For CAP input–output analysis, the averaged waveform was manually inspected for the first negative amplitude deflection after stimulus onset.

PSTRs were measured and analyzed as described.[38] The PSTR stimulus, a 200 ms pseudo-randomized noise burst with a 2.5 ms ramp, was presented with alternated polarity and 100 iterations. The noise had a center frequency of 5.6, 8, 11.3, 16, or 22.6 kHz and a bandwidth of 1/3 of an octave. The intensity ranged from 10 to 80 dB SPL in 10 dB steps. The ISI was 420 ms, and the recording window was 410 ms long. The signal was hardware filtered (bandwidth with 1 kHz high pass and 30 kHz low pass, and the signal was amplified by factor 5000. For analysis, the two electrical recordings within each polarity pair were averaged for isolation of the neurophonic signal. The signal was digitally bandpass filtered with 300–1200 Hz, rectified, and finally smoothed (window of 1 ms). For further analysis, the maximum amplitude within the first 30 ms after stimulus onset (peak) and the average of the amplitude within the last 30 ms before stimulus offset (plateau) were calculated and used for determination of the peak/plateau ratio.

2.8 | Cortical local field potentials

Eight control mice and nine *Bdnf*^{Pax2} KO mice were anesthetized (see above); the fur in the surgical area was removed, and the skin was disinfected with Octenisept® (Schülke & Mayr GmbH, Norderstedt, Germany). 20–40 µL Xylocaine 2% (AstraZeneca, Wedel, Germany) was applied subcutaneously at sites of surgical incisions for local anesthesia, and the mice were laid on a pre-warmed resting pad (37°C). Breathing was monitored and supported by oxygen supply. The skin was cut ~12 mm with a scalpel, and connective tissue was removed from the surface of the skull. A 0.6 mm hole was drilled in the

skull 1 mm posterior to lambda. A handmade silver wire electrode (0.125 mm) insulated by varnish and silicone and ending in a small silver bead was placed within the niche and glued with Histoacryl (B. Braun, Melsungen, Germany) was used as a reference electrode.

Two electrodes similar to the previous one were placed on the cortex's surface after drilling holes above the right PFC (0.2 mm lateral and 2 mm anterior to bregma) and the left V1 (2.5 mm lateral and 2 mm posterior to bregma). For local field potentials of the right AC (4 mm lateral, 3 mm posterior, and 2 mm ventral to bregma) and the left HC (1.5 mm lateral, 2 mm posterior, and 1.3 mm ventral to bregma), a 1 mm drill was used and the 0.125 mm silver wires were inserted and glued into 27G cannulas used as guiding shafts. Again, the electrodes were glued with Histoacryl to the edges of the drilling hole. All coordinates for the electrodes were chosen according to the mouse brain atlas,[36] and the electrode positions were verified ex vivo in brain slices stained either using toluidine blue or the staining protocol used for double detection of mRNA and protein[37] (Figure S1). All electrodes were connected to an active head stage (LabRat AC16LR, Tucker Davis Technologies, Alachua, FL, USA). The signal was transferred to a programmable gain amplifier (PGA16 Rev.B, Multichannel Systems MCS, Reutlingen, Germany). The PGA, supporting frequency bands between 5 Hz to 5 kHz, was used for 5000x amplification. The PGA was connected to a multi-I/O measurement card (NI PCIe-6321, National Instruments, Austin, TX, USA) housed in a personal computer.

2.9 | Resting-state activity

The ~17.3 min of resting-state recording were subdivided into ~1000 epochs with a duration of 1 s. The Fourier transform of each epoch was computed using the FFT function of Matlab (version R2021b). Afterward, the absolute value of the FFT of all epochs was averaged. The final step was to compute the genotype group averages.

2.10 | Auditory-evoked potentials

For measurements of auditory-evoked potentials, pure-tone frequency stimuli were presented at either 5.6, 11.3, or 22.7 kHz with an intensity of ~90 dB SPL. To compare the evoked signals with baseline activity, another recording without a stimulus was performed. The repetition rate for each stimulus condition was 2000, the stimulus length was 100 ms, and the recording interval was 507 ms.

For all cortical measurements of ASSR, a carrier of 11.3 kHz was chosen. For the I/O function, the carrier was modulated by frequencies of either 10, 40, or 128 Hz at 100% modulation depth. For each modulation frequency, the stimulus was presented at intensities from 10 to 90 dB SPL in 10 dB steps. For the modulation transfer function, the carrier was modulated by 5, 10, 16, 20, 32, 40, 64, 80, 128, 160, 256, 320, 512, 640, 1024, 1280, and 2048 Hz at 100% modulation depth. The stimulus intensity was 90 dB SPL. The repetition rate for each ASSR stimulus condition was 64, the stimulus length was 1000 ms, and the recording interval was 1207 ms.

2.11 | Golgi–Cox staining

Brains of 10- to 12-week-old mice were dissected and stained according to the manufacturer's guidelines using the FD Rapid GolgiStain Kit (FD NeuroTechnologies, Columbia, MD, USA). In brief, dissected brains were immersed in A:B solution for 10 days at room temperature in the dark. Brains were transferred to solution C and kept in the dark for three more days. Afterward, coronal vibratome sections were made (VT1000S, Leica, Wetzlar, Germany) at a thickness of 150 µm and mounted on gelatin-coated microscope slides (FD NeuroTechnologies). The sections dried overnight at room temperature in the dark and were stained according to the manufacturer's guidelines. For embedding, Eukitt Quick-hardening mounting medium (Sigma-Aldrich, Darmstadt, Germany) was used.

Individual pyramidal neurons of the hippocampal CA1 region were included for analysis if (i) completely impregnated and (ii) the integrity of the dendritic branches was preserved. The first dendritic branch from the main apical shaft was analyzed if uninterrupted by other dendrites and at least 20 µm long. *Z*-stack images were acquired using an upgraded Olympus BX61 microscope (EVIDENT Europe GmbH, Hamburg, Germany) with 60× magnification. On average, four to eight neurons were included per animal for each brain region.

3 | QUANTIFICATION AND STATISTICAL ANALYSIS

3.1 | Statistics and numbers

All statistical information, including the statistical tests and post hoc tests used, the exact value of n, what n represents and the precision documentation of statistical outcome, can be found in Table S1. In brief, data were tested for normal distribution (Shapiro–Wilk normality test, $\alpha = 0.05$). Differences between the means were compared for statistical significance by unpaired two-tailed Student's t-test (parametric) and Mann–Whitney U

test for parametric and non-parametric data, respectively. Multivariate sample mean differences were tested by permutation test and 2-way ANOVA or MANOVA for non-parametric and parametric data, respectively. The Bonferroni–Holm method was used to correct for type I error.

In the figures, significance is indicated by asterisks (*$p < .05$, **$p < .01$, ***$p < .001$, and ****$p < .0001$); n.s. denotes non-significant results ($p > .05$). A trend is indicated by asterisk in brackets [(*) $p < .1$].

3.2 | Electrocochleographic recordings

Thresholds were determined from individual ears from averaged waveform responses as the lowest SPL resulting in a signal visually distinguishable from noise. For CAP I/O analysis, the averaged waveform was visually inspected for the first negative amplitude deflection after stimulus onset. The latency of the CAP was registered for each stimulus intensity for each individual ear, and the resulting growth function was averaged and presented as the mean and SEM. PSTR peak/plateau ratios were averaged for all animals within the group and presented as mean and SEM.

3.3 | Cortical local field potential analysis

Field potential analysis comprised resampling with the eeglab anti-aliasing filter cutoff function (rate 3000 Hz, cutoff 0.8, band width 0.2), artifact detection and rejection by a variance–amplitude criterion, rejecting the 5% trials with the highest variance, segmentation and transformation of the first 100 of 120 ms stimulus duration (ISI 387 ms) into frequency space by FFT (rectangular window), compute evoked responses be simple time domain averaging, peak-to-peak (min/max within predefined time interval) analysis of voltage values, separating evoked and induced oscillations by phase-coherent/phase-incoherent averaging, and computation of peak-to-peak (min/max within predefined time interval). The frequency bands were analyzed for the following bands: alpha (8–15 Hz, including 5–7 Hz theta band), beta (15–25 Hz), low gamma (25–35 Hz), mid gamma (35–65 Hz), and high gamma (65–125 Hz); results were tabulated and statistically evaluated by permutation analysis confining data permutation to individual setups, and non-parametric signed-rank testing across genotypes for individual frequency bands and stimulus conditions (4.66, 5.66, 6.66, 10.3, 11.3, 12.3, 21.7, 22.7, and 23.7 kHz). For the statistical analysis, the 9 stimulus frequencies were grouped into low (4.66, 5.66, and 6.66 kHz), mid- (10.3, 11.3, and 12.3), and high (21.7, 22.7, a 23.7 kHz) frequencies. The peak-to-peak amplitude stimulus frequency regions were analyzed similarly to the ASSR via permutation, while ensuring that only measurements from the same setup were permuted.

3.4 | Dendritic spine analysis

Spine analysis and classification were conducted as previously described,[39] using the Reconstruct software (http://synapses.clm.utexas.ed). Briefly, all protrusions that were in direct contact with a given segment of a dendrite were counted as spines. Segments of at least 30 µm long were analyzed for each dendrite. Spine density was calculated as the number of protrusions per µm. The length and the width of spines were then transferred to a spreadsheet.[39]

3.5 | Fluorescence analysis of brain immunohistochemistry

Z-stacks were analyzed using the free software ImageJ (NIH, Bethesda, MD, USA). For each *z*-stack, the three channels (PV, vGlut1, and DAPI) were split and analyzed separately as a maximum intensity projection over the *z*-axis. A binary mask was created using the default parameters, and then, a ROI (270 × 270 pixels for 1024 × 1024 images and 540 × 540 pixels for 2048 × 2048 images) was placed on the dendrites of the pyramidal neurons in each single-channel picture. Afterward, the average fluorescence intensity within the ROI was calculated. For analysis, the data were normalized between groups in order to account for variability in staining. For each individual animal (ten control mice and 12 *Bdnf*^{Pax2} KO mice), one slice was processed, imaged, and between 3 and 5 pictures were analyzed, the average of which was then used for further statistical analyses.

4 | RESULTS

4.1 | Bdnf^{Pax2} KO mice exhibit reduced auditory-evoked local field potentials

To determine whether *Bdnf*^{Pax2} KO mice exhibit cortical activity changes with characteristics of an autism phenotype, sound-evoked LFPs were recorded in adult *Bdnf*^{Pax2} KO and control mice in response to pure-tone stimuli between 4 and 23 kHz at 90 dB SPL from the AC, HC, PFC, and V1 (Figure 1; Figure S1; for statistics, see Table S1).

When evoked LFP amplitudes were compared between the two groups in response to 5, 11, and 22 kHz stimuli,

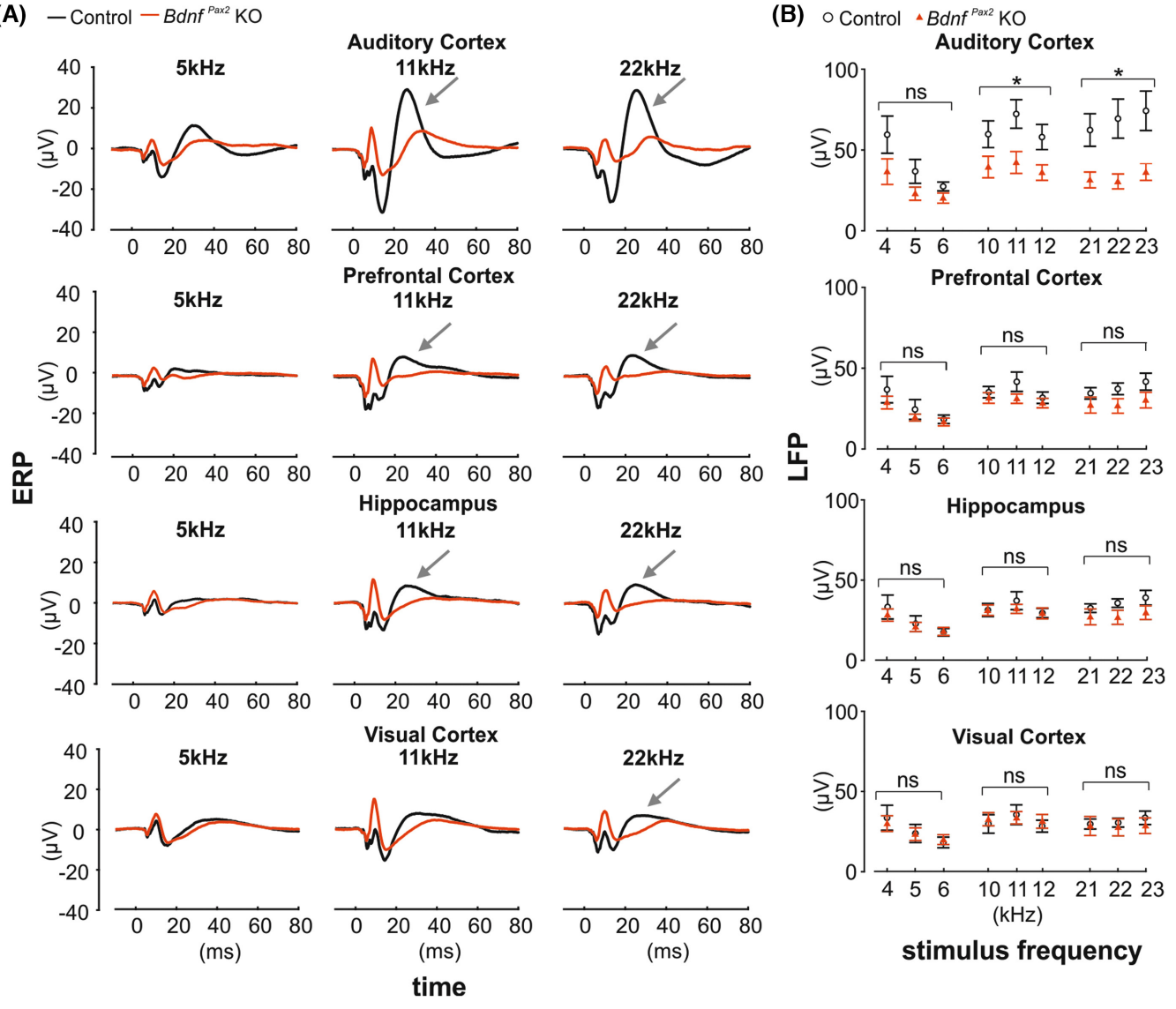

FIGURE 1 Reduced LFP amplitudes in response to auditory stimuli of best frequencies in *Bdnf*^{Pax2} KO mice. (A) Traces of event-related potentials averaged from evoked responses of 8 control and 9 *Bdnf*^{Pax2} KO mice for three different stimulus frequencies: 5 kHz (left panels), 11 kHz (middle panels), and 22 kHz (right panels) for the auditory cortex (1st row), prefrontal cortex (2nd row), hippocampus (3rd row), and visual cortex (bottom row). Controls: black curves; *Bdnf*^{Pax2} KO: red curves. (B) Group data of peak-to-peak amplitude of single ERPs for controls (black) and *Bdnf*^{Pax2} KOs (red) based on the first 50 ms of the ERP (LFP amplitude) in response to stimuli presented in groups of frequencies ranging from ca. 4–6, 10–12, and 21–23 kHz (abscissa). Gray arrows in (A) indicate the LFP. Data in (B) present mean ± SEM. *$p < .05$, ns $p \geq .05$. Detailed statistical information can be found in Table S1.

it became evident that control mice exhibited a strong event-related potential (ERP) in the AC in response to 11 and 22 kHz auditory stimuli and a much weaker one in response to 5 kHz stimuli, whereas *Bdnf*^{Pax2} KO mice had weak ERPs in the AC and the other brain regions in response to all frequencies (Figure 1A). No significant amplitude differences were seen in the PFC, HC, or V1 (Figure 1A).

To further classify evoked LFP responses over the hearing range, LFP amplitudes were plotted against stimulation frequencies (Figure 1B). *Bdnf*^{Pax2} KO mice exhibited significantly lower evoked response amplitudes in the AC in comparison with controls, particularly in the best hearing range (i.e., 10–12 kHz) up to the extended frequency range (i.e., 21–23 kHz), most critical for communication and behavior[40,41] (Figure 1B; Table S1). In PFC, HC, and V1, no significant difference was detected for LFP amplitudes in response to any presented frequency (Figure 1B; Table S1).

Taken together, a gradual increase in sound-evoked LFP amplitudes in response to acoustic stimuli in the range of best hearing frequencies in mice (> 10 kHz) is seen in the AC, but not in PFC, HC, or V1. In *Bdnf*^{Pax2} KO mice, the sound-evoked LFPs in response to >10 kHz were significantly reduced in the AC, suggesting, when

considering principles of evoked LFP,[42] that the *Bdnf*^{Pax2} KO mice display a profound impairment of input and output intracortical network activity.

4.2 | *Bdnf*^{Pax2} KO mice exhibit reduced evoked and induced ASSRs and increased spontaneous oscillations

To further determine whether the source of the reduced sound-evoked LFP responses in *Bdnf*^{Pax2} KO mice stems from cortical or subcortical nuclei, we analyzed the signal envelope following responses to amplitude-modulated stimuli (ASSRs). ASSRs reflect the summation of phase-locked activity from multiple generators of neural stimuli within the auditory system, including the cochlea, auditory nerve, IC, and AC.[43] The contributions of ASSR sources in response to lower (10–40 Hz) modulation rates are dominated by cortical components,[43] while ASSRs in response to higher (>100 Hz) modulation rates are dominated by subcortical components.[43]

Modulation frequencies between 5 and 2048 Hz were used at an 11.3 kHz carrier frequency. ASSR amplitudes were depicted for 100% modulation depth at 90 dB SPL and plotted against the frequency oscillation bands (Figure 2; Figure S2). Evoked ASSR activity reflects bottom-up sensory transmission primarily by driving inputs.[43] This evoked ASSR activity was distinguished from induced ASSR activities, which are not strictly locked to stimulus onset and rather represent internal dynamics of cortical networks related to higher cognitive functions.[30,43] As shown for the AC (Figure 2A), PFC (Figure 2D), HC (Figure S2A), and V1 (Figure S2D), evoked and induced ASSR amplitudes were significantly reduced in *Bdnf*^{Pax2} KO mice in response to 10-, 40-, and 128 Hz-modulated tones and remained significantly diminished in comparison with control mice up to 320 Hz modulation frequency (see dashed lines in Figure 2A,D; Figure S2A,D).

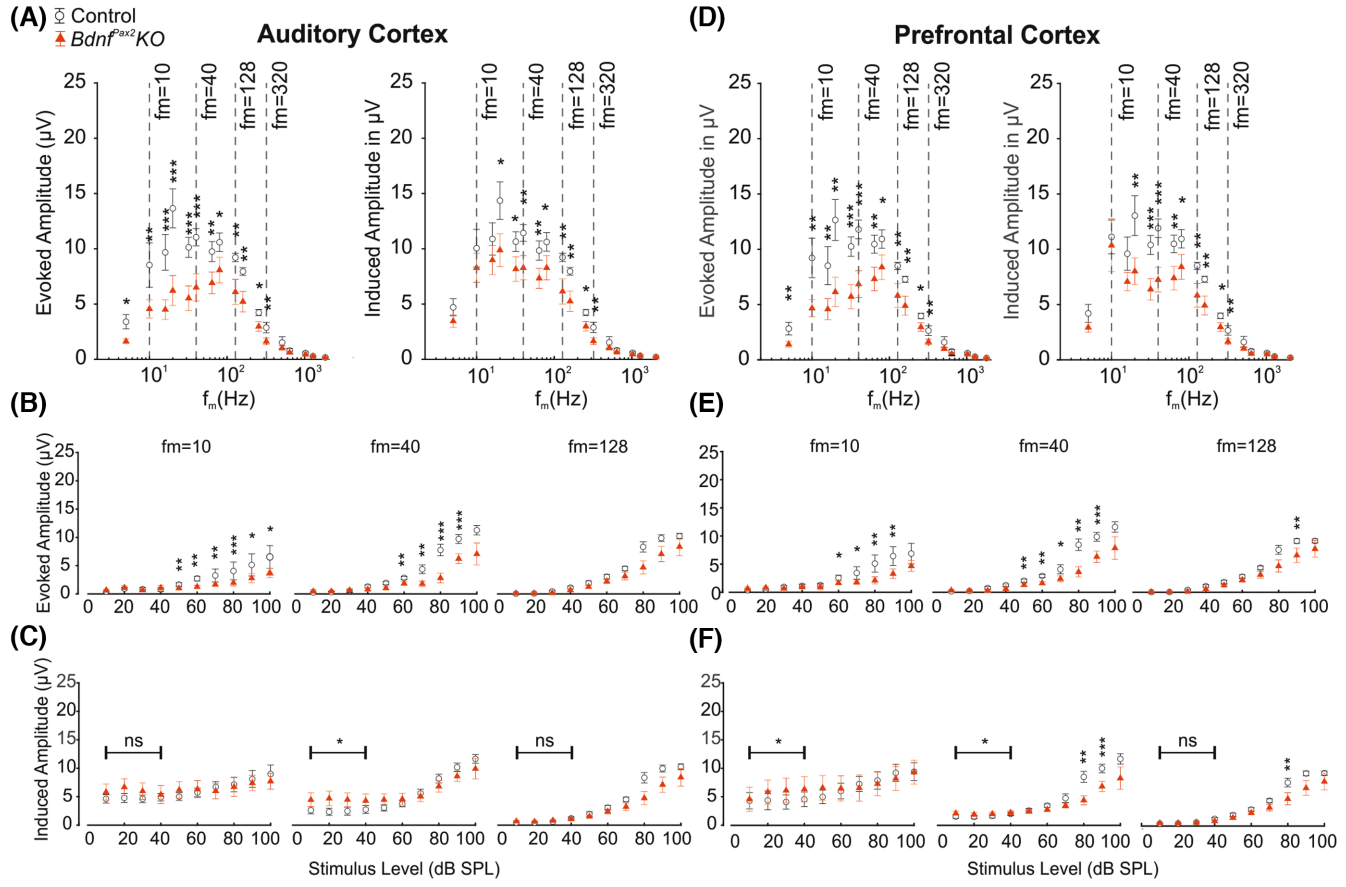

FIGURE 2 Averaged evoked and induced ASSR response amplitude in cortical regions of control and *Bdnf*^{Pax2} KO mice. Distribution of evoked and induced response amplitude measured at different modulation frequencies (f_m) in the (A) auditory cortex and (D) prefrontal cortex (controls: black circles; *Bdnf*^{Pax2} KO: red triangles). Distribution of (B,E) evoked and (C,F) induced response amplitudes in response to increasing SPL of the stimuli for the (B,C) auditory cortex and (E,F) prefrontal cortex. Left panels in (B,C,E,F) show 10 Hz f_m, middle panels 40 Hz f_m, and right panels 128 Hz f_m. Mean ± SEM of 8 control and 9 *Bdnf*^{Pax2} KO mice. *$p < .05$, **$p < .01$, ***$p < .001$. Detailed statistical information can be found in Table S1.

These reduced evoked and induced ASSR amplitudes in AC, PFC, V1, and HC suggest an impaired summation of phase-locked activity from subcortical and cortical regions in *Bdnf*^{Pax2} KO mice that have impacted cortical networks related to the AC.

To better explain the reduced ASSR amplitudes in *Bdnf*^{Pax2} KO mice, we analyzed the dependence of the ASSR amplitude on stimulus intensity. This could shed light on deficits in a specific type of ANF. The high-spontaneous rate (high-SR) low-threshold ANFs dominate the encoding of the envelope of amplitude-modulated tones at low sound intensities in the best frequency range and contribute at higher sound intensities through activation of sidebands of neurons with characteristic frequencies outside of best frequency range.[44]

ASSR amplitudes were plotted against increasing sound intensities from 10 to 100 dB SPL and specifically analyzed for 10-, 40-, or 128 Hz-modulated tones (Figure 2B,E; Figure S2B,E). In the AC, control mice exhibited a characteristic increase in response amplitude with increasing stimulus intensity (>50 dB SPL) for 10- and 40 Hz-modulated tones. This effect was significantly less pronounced in *Bdnf*^{Pax2} KO mice (Figure 2B; Table S1).

In both control and *Bdnf*^{Pax2} KO mice, ASSR amplitudes in the PFC, HC, and V1 showed a progression identical to the respective AC response, particularly to the higher SPL range. This points to a coherence between 10 and 40 Hz activity within these brain regions in response to higher intensity sound (Figure 2B,E; Figure S2B,E). The induced (non-phase-locked) responses were slightly higher in *Bdnf*^{Pax2} KO mice compared to controls specifically for low sound intensities in response to 40 Hz-modulated tones in the AC (Figure 2C; Table S1) and PFC (Figure 2F; Table S1) and in response to 10 Hz-modulated tones in the PFC (Figure 2F). This effect was not present in the HC or V1 (Figure S2C,F; Table S1).

In summary, *Bdnf*^{Pax2} KO mice exhibit diminished evoked ASSR amplitudes at higher sound intensities, best explained through missing high-SR ANF-driven activation outside of neurons' characteristic frequency. Furthermore, we find slightly elevated induced ASSR amplitudes at lower sound intensities in *Bdnf*^{Pax2} KO mice, best explained through missing high-SR ANF-driven activation in neurons' best frequency range. Overall, this characteristic response profile suggests that *Bdnf*^{Pax2} KO mice exhibit disturbed high-SR ANF function, preventing them from properly contributing to the ASSR amplitude.

If the cause of reduced sound-evoked cortical LFPs and diminished evoked ASSRs in *Bdnf*^{Pax2} KO mice is of subcortical origin, we would expect spontaneous LFPs (independent of stimuli) to be elevated in *Bdnf*^{Pax2} KO mice, as intracortical network activity is modulated indirectly through elevated subcortical baseline activity.

To elucidate this, spontaneous cortical activity was measured in the AC, PFC, HC, and V1 in *Bdnf*^{Pax2} KO mice and controls (Figure 3). In the AC, the spontaneous activity of *Bdnf*^{Pax2} KO mice was significantly higher than that of controls in the alpha (5–15 Hz), beta (15–25 Hz), low-gamma (25–35 Hz), and high-gamma (35–65 Hz) bands (Figure 3A; Table S1). Interestingly, the spontaneous LFP power was also elevated, although less prominently, in the PFC in the alpha, beta, and low-gamma bands (Figure 3B; Table S1) and in the V1 in the beta and low-gamma bands (Figure 3D; Table S1). No significant differences were found in the HC (Figure 3C; Table S1).

Conclusively, diminished evoked ASSR at higher sound intensities, elevated induced ASSR at lower sound intensities, and elevated LFPs at rest in *Bdnf*^{Pax2} KO mice all suggest that the spontaneous ongoing activity at the input site of intracortical networks in the AC has changed. This may influence the operation point for feed-forward synchronization and self-organizing intracortical induced synchronization, both required for proper evoked and induced brain oscillations.

4.3 | *Bdnf*^{Pax2} KO mice exhibit reduced evoked and enhanced induced alpha, beta, and gamma oscillations in cortical regions

As autism is suggested to be a "critical period" disorder,[3,4] we hypothesized that elevated spontaneous LFP activity in *Bdnf*^{Pax2} KO mice is associated with a cortical inhibitory component that failed to mature during the critical period after hearing onset. This could result from underdeveloped near-threshold auditory processing as concluded from the aforementioned results.

If this were the case, we would expect a particularly profound impact on the alpha and beta neuro-oscillatory bands, as they are generated earlier than the higher frequency gamma bands in humans and rodents, coinciding with the differential onset of sensory modalities driven by the establishment of PV-IN networks.[5,10]

We therefore tested specific frequency-band power differences in response to sound frequencies increasing from 4 to 23 kHz in *Bdnf*^{Pax2} KO and control mice. Evoked and induced LFP responses to increasing stimulus frequencies are distinguished and shown for each neuro-oscillatory frequency band separately in the AC (Figure 4), PFC, HC, and V1 (Figure S3) of *Bdnf*^{Pax2} KO mice and controls. In comparison with controls, *Bdnf*^{Pax2} KO mice exhibited significantly lower evoked LFP responses in the alpha, beta, and low-gamma bands, particularly in response to higher

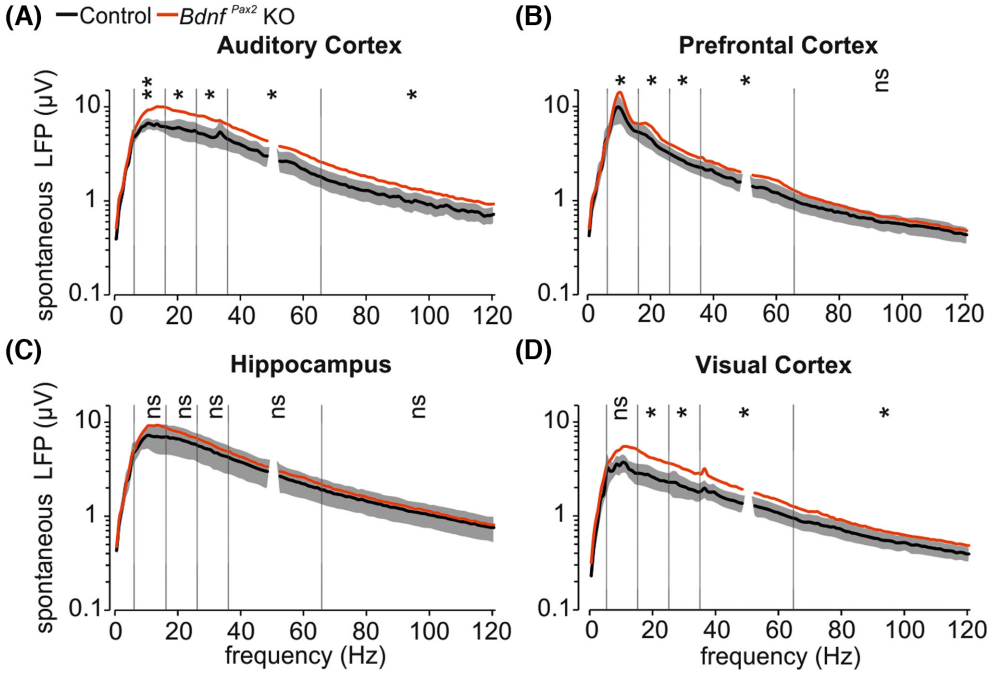

FIGURE 3 Elevated spontaneous LFP power in cortical regions of $Bdnf^{Pax2}$ KO mice. Power spectra for LFP in frequency oscillation bands alpha (5–15 Hz), beta (15–25 Hz), low gamma (25–35 Hz), mid-gamma (35–65 Hz), and high gamma (65–125 Hz), separated by vertical lines. The spontaneous LFP power was significantly higher in cortical regions of $Bdnf^{Pax2}$ KO mice (red lines) as compared to controls (black lines) (A, auditory cortex, B, prefrontal cortex, and D, visual cortex). (C) In the hippocampus, the higher spontaneous LFP power does not reach statistical significance in the analyzed frequency bands. The 50 Hz powerline interference has been removed (gap). Spectral power decreases below 10 Hz due to bandpass filtering (>10 Hz–5 kHz with 60 dB attenuation per decade). Controls: black curves; $Bdnf^{Pax2}$ KO: red curves. Mean ± 95% confidence range of 8 controls and mean of 9 $Bdnf^{Pax2}$ KO mice. $^{*}p < .05$, $^{**}p < .01$, ns $p \geq .05$. Detailed statistical information can be found in Table S1.

sound frequencies (>6 kHz) (Figure 4A–C; Table S1). This effect was less prominent in the mid-gamma band (Figure 4D; Table S1) and not present in the high-gamma band (Figure 4E; Table S1). This indicates that sound-evoked EEG power is diminished across a wide range of frequency bands in $Bdnf^{Pax2}$ KO mice.

Although the amplitude sound-evoked LFP was significantly lower only in the AC of $Bdnf^{Pax2}$ KO mice (Figure 1), when the evoked LFP was divided into specific oscillatory frequency bands, differences in other brain regions became apparent. In the PFC, HC, and V1, $Bdnf^{Pax2}$ KO mice exhibited significantly lower evoked LFPs compared to controls mainly in alpha and beta bands and particular for stimulation frequencies above 6 kHz (Figure S3; Table S1).

Induced LFPs were also examined across different oscillatory frequency bands and overall stimulus frequencies. In the course of this analysis, $Bdnf^{Pax2}$ KO mice exhibited higher induced LFPs in comparison with controls particularly in the AC, PFC, and V1 in the beta band (Figure 4; Figure S3; Table S1).

This indicates that the diminished sound-evoked EEG power across <65 Hz frequency bands in the AC and in alpha- and beta-frequency bands in the PFC, HC, and V1 of $Bdnf^{Pax2}$ KO mice is at least partially accompanied by an enhancement of induced LFP power in the AC, PFC, and V1 in the beta band. Here, an association with the increased ongoing activity of induced ASSR responses to low-SPL stimuli in the AC and PFC becomes apparent. In both cases, elevated spontaneous feed-forward synchronization may have influenced self-organizing intracortical induced synchronization.

4.4 | $Bdnf^{Pax2}$ KOs exhibit deficits in synchronized responses and high-SR ANF processing

Thus far, all results would be in line with an immaturity of high-SR ANFs in $Bdnf^{Pax2}$ KO mice. High-SR ANFs develop during the critical time period after hearing onset, nearly independent of basic hearing function.[45,46] They define the perceptual hearing thresholds at behaviorally relevant frequency regions[47,48] and contribute to level-dependent response properties.[49] High-SR ANFs have a high synchronicity and phase-locking capacity[44] and thus contribute to both ASSRs and the CAP amplitude of the auditory nerve.[50,51]

Thus, as an indicator for ANF functionality, the CAP signals were recorded at the round window of

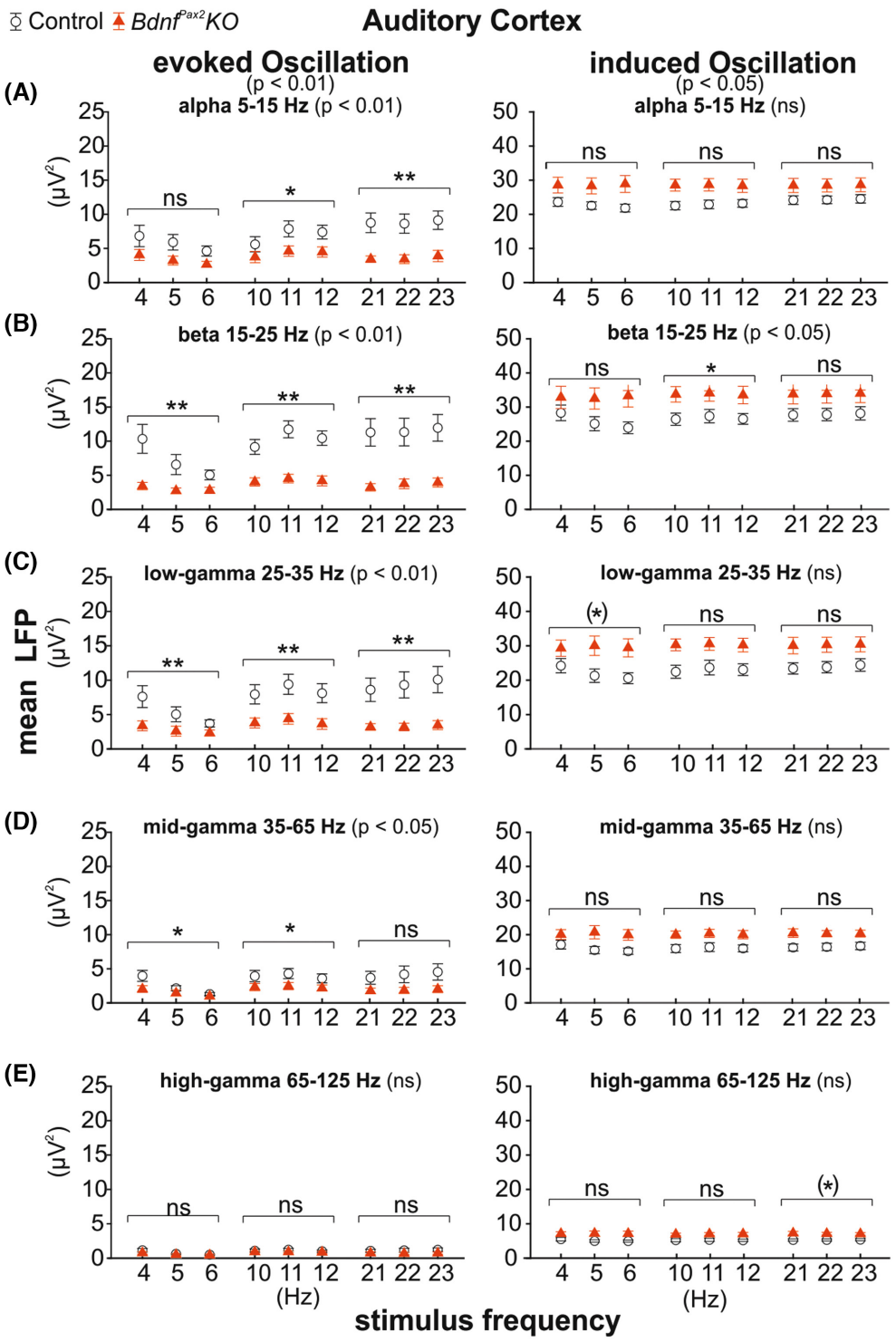

FIGURE 4 Reduced evoked and elevated induced LFP power at alpha, beta, and low-gamma bands in the AC of *Bdnf*^{Pax2} KO mice. Evoked (left panels) and induced (right panels) oscillation power (mean LFP in μV^2) in response to low- (4–6 kHz), middle- (10–12 kHz), and high-frequency stimuli (21–23 kHz). The effect of stimulus frequencies on (A) alpha oscillations (5–15 Hz), (B) beta oscillations (15–25 Hz), (C) low-gamma oscillations (25–35 Hz), (D) mid-gamma oscillations (35–65 Hz), and (E) high-gamma oscillations (65–125 Hz) were compared in the respective frequency group between control and *Bdnf*^{Pax2} KO mice. Evoked oscillations in *Bdnf*^{Pax2} KO mice (red triangles) were smaller in the lower oscillatory bands (A–D, left), black empty circles), most consistently at stimulus frequencies around 11 kHz. Induced oscillations (right) were higher in *Bdnf*^{Pax2} KO mice in comparison with controls, though the difference reached statistical significance only for the beta oscillatory band (B, right). Controls: black empty circles; *Bdnf*^{Pax2} KO: red triangles. Mean ± SEM of 8 control and 9 *Bdnf*^{Pax2} KO mice. *$p < .05$, **$p < .01$, ns $p \geq .05$, and $^{(*)}p < .05$ uncorrected for multiple testing. Detailed statistical information can be found in Table S1.

anesthetized *Bdnf*^{Pax2} KO mice and controls (Figure 5A). CAP thresholds showed significant differences between *Bdnf*^{Pax2} KO and control mice at frequencies below 11 kHz (Figure 5B; Table S1); these differences mirror the differences in auditory brainstem response thresholds reported in previous studies.[33] Interestingly, when analyzed in a threshold-normalized manner, the CAP amplitudes in response to click stimuli were lower in *Bdnf*^{Pax2} KO mice at all sound intensities (Figure 5C, left; Table S1), while the latency was unaffected (Figure 5C, right; Table S1).

When amplitude growth functions were measured for different frequencies ranging from 2 to 32 kHz, *Bdnf*^{Pax2} KO mice displayed lower CAP amplitudes at frequencies between 8 and 32 Hz (Figure 5F–J; Table S1). Addressing frequency gradients, CAP amplitudes of all measured frequencies were compared at 20 dB above threshold (Figure 5K). Again, CAP amplitudes of *Bdnf*^{Pax2} KO mice were significantly lower in response to stimuli at and above the best hearing frequency range (Figure 5K; Table S1). Notably, stimuli of this same frequency range also elicited lower evoked cortical brain activity in *Bdnf*^{Pax2} KO mice (Figure 1, Figure 4). Similar effects were observed when comparing CAP amplitudes of all frequencies at 30 (Figure 5L; Table S1) and 40 dB above threshold (Figure 5M; Table S1).

The significantly reduced CAP amplitudes around the best frequency ranges in *Bdnf*^{Pax2} KO mice may suggest an inability to properly phase lock and synchronize summed spike activity. As a result, when action potentials are out of phase, this desynchronization destructively adds to the CAP amplitude, which is defined through the summation of all synchronized action potentials.

High-SR ANFs, rather than low-spontaneous rate (low-SR) high-threshold ANFs, were previously shown to be the primary contributor to phase locking and synchronization of auditory nerve activity.[50] The proportion of high-SR ANFs to low-SR ANFs can be evaluated by measuring PSTRs. Noise-band stimuli in alternating polarity were presented, and the electrical signal was recorded at the round window; then, the responses were averaged in pairs.[38] Using a bandpass filter, the neurophonic response was isolated, then rectified, and averaged across all repetitions (Figure 6A). The PSTR has an envelope shape (Figure 6B) similar to the peristimulus time histograms derived from single-fiber recordings of ANFs. The envelope consists of a synchronized response at the onset of stimulation followed by an alternating current component arising from a phase-locked activity of ANFs to stimulus envelope fluctuations.[38,52] The peak-to-plateau ratio, which reflects the proportion of high- to low-SR ANFs, was calculated for all traces and then compared in a threshold-dependent manner.

Bdnf^{Pax2} KO mice and controls did not differ in their peak-to-plateau ratio for low- to mid-frequency stimuli (i.e., below 11.3 kHz) (Figure 6C–E; Table S1). At higher frequencies (i.e., 16 and 22 kHz), however, *Bdnf*^{Pax2} KO mice had a significantly smaller peak-to-plateau ratio in comparison with controls (Figure 6F,G; Table S1). When the peak-to-plateau ratio was compared at all frequencies at 30 dB above threshold, an overall significantly reduced ratio was found in *Bdnf*^{Pax2} KO mice (Figure 6H; Table S1).

Conclusively, the lower CAP amplitude along with the lower peak-to-plateau ratio observed predominantly in high frequencies in *Bdnf*^{Pax2} KO mice point to a deficit in high-SR ANF function that leads to failed maturation of precise spike synchronization. This high-SR ANF deficit alone may explain the stark reduction in evoked cortical LFPs in the AC, linked to reduced evoked power in the alpha, beta, and low-gamma bands, typical for an autism-like phenotype. This would lead us to expect in *Bdnf*^{Pax2} KO also structural changes in cortical and associated regions linked to E/I imbalance, comparable to what has been observed in autistic phenotypes.

4.5 | *BDNF*^{Pax2} KO mice exhibit impaired spine maturation and PV-IN levels

Reduced cortical inhibition, leading to E/I imbalance in neuropsychiatric diseases, was associated with changes in GABAergic proteins and spine maturation patterns, for example, in the HC (e.g.,[53–55]).

Consistent with the notion that cortical brain activity changes in *Bdnf*^{Pax2} KO mice are a consequence of altered driving force stemming from the periphery of the cochlea rather than resulting directly from cortical network changes, we want to highlight the previous finding of similar cell counts of PV-INs and similar BDNF mRNA levels in the AC and HC in *Bdnf*^{Pax2}KO mice and controls (Figure S4A-C, with the permission of Front Mol Neurosci[20]). However, PV-IN labeling in the neuropil domain in layer III/IV of the AC, the stratum radiatum, and the stratum lucidum of hippocampal CA1/CA3 regions of *Bdnf*^{Pax2} KO mice showed reduced PV-IN levels. This coincided with significantly higher Arc mRNA levels in the same regions (Figure S4D,E; with the permission of Front Mol Neurosci[20]).

In the present study, the structural correlate of enhanced cortical and hippocampal excitability in *Bdnf*^{Pax2} KO mice was validated by measuring the expression of PV protein and vGlut1 protein as markers of inhibitory and excitatory synapses, respectively, in combination with spine maturity, as described.[56] Images in Figure 7 were taken of the stratum radiatum (Figure 7A), a hippocampal region where the Schaffer's collaterals contact the dendrites of CA1 pyramidal

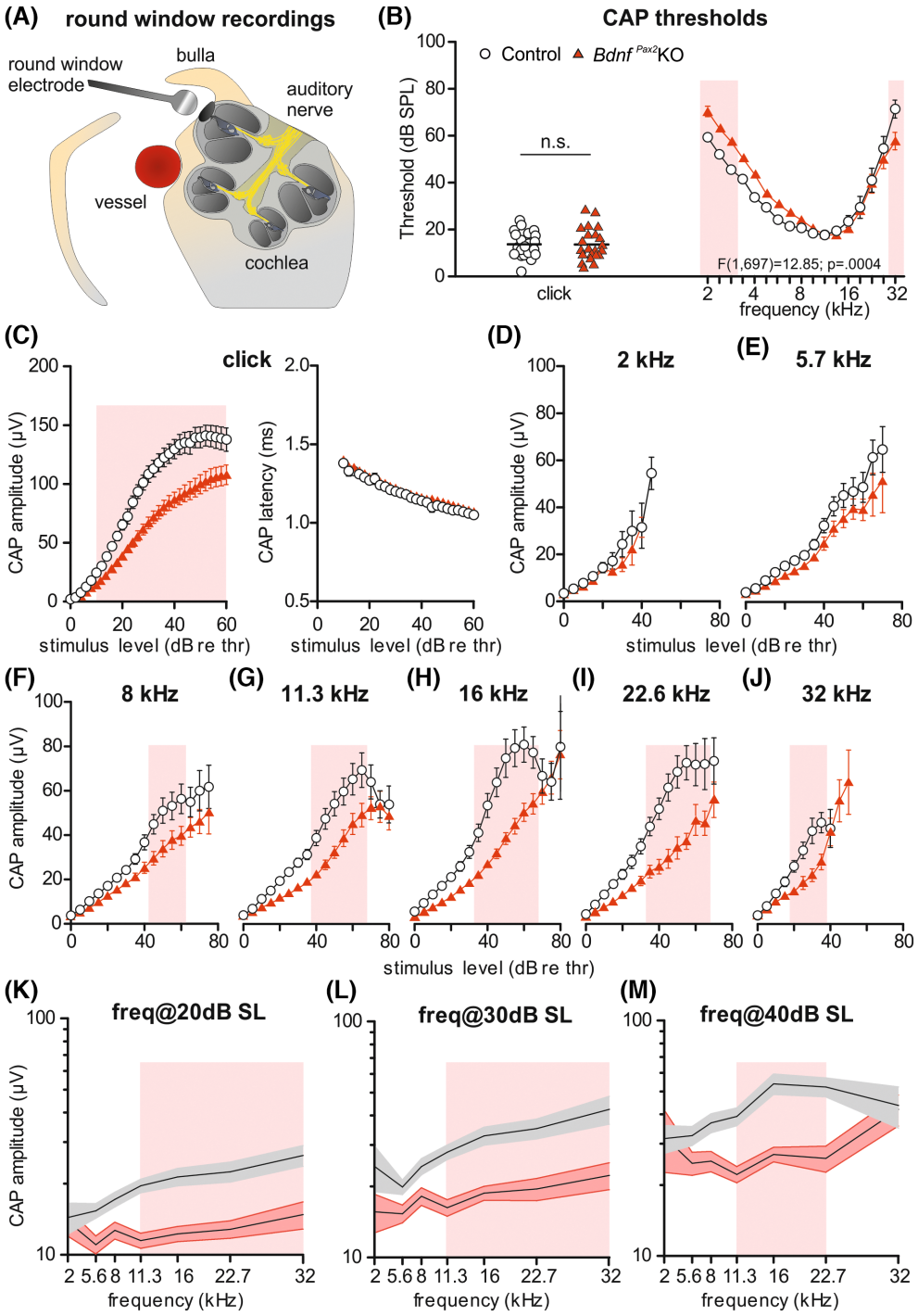

FIGURE 5 Reduced compound action potentials (CAP) in *Bdnf*^{Pax2} KO mice. (A) Schematic drawing of electrode placement for electrocochleography at the round window. (B) Click- and pure-tone frequency stimulus-evoked CAP thresholds. (C) Click-evoked threshold-normalized CAP input/output growth-function amplitude (left panel) and latency (right panel). (D) Threshold-normalized CAP input/output growth-function amplitude elicited with pure-tone stimuli at 2 kHz, (E) 5.7 kHz, (F) 8 kHz, (G) 11.3 kHz, (H) 16 kHz, (I) 22.6 kHz, and (J) 32 kHz. (K) Comparison of CAP signals for all frequencies at a similar intensity of 20 dB above threshold, (L) 30 dB above threshold, and (M) 40 dB above threshold. (B) Left panel = individual ears (single dots). (B–M, right panel) = mean ± SEM. Red highlights indicate significance in post hoc comparison. ns $p \geq .05$. Detailed statistical information can be found in Table S1.

neurons. *Bdnf*^{Pax2} KO mice exhibited significantly lower PV fluorescence levels (Figure 7 B,C; Table S1) and significantly higher vGlut1 fluorescence levels in comparison with controls (Figure 7B,C; Table S1).

Golgi's staining was performed on hippocampal brain slices in order to visualize dendritic spines (Figure 7D). *Bdnf*^{Pax2} KO mice exhibited higher spine density, defined as the number of protrusions per μm

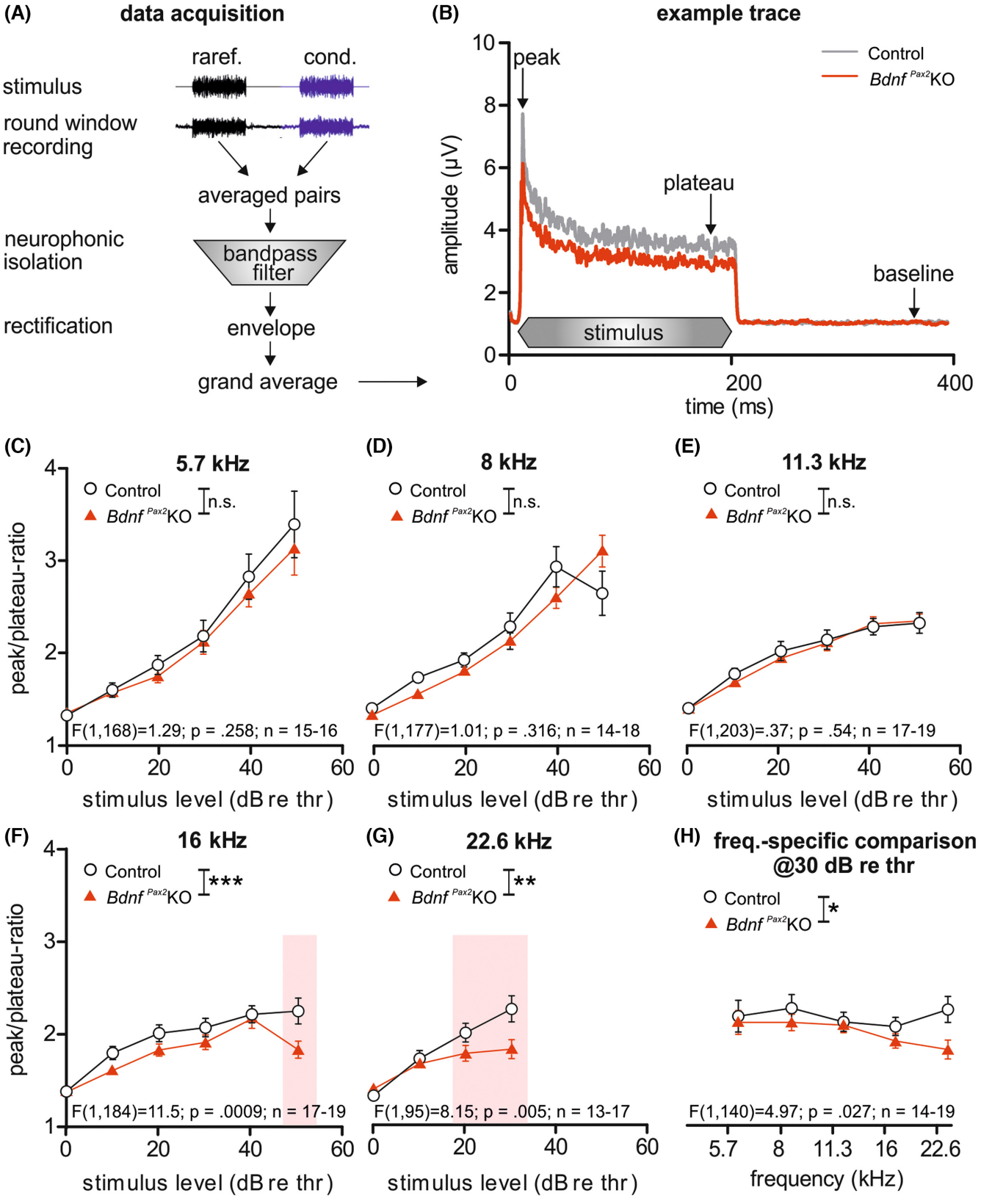

(Figure 7E). In addition, the length-to-width ratio, reflecting different spine morphology, was higher in *Bdnf*^{Pax2} KO mice, indicating longer, thinner spines (immature spines) in comparison with controls (Figure 7F-H). Overall, the decreased PV and increased vGlut1 levels along with an immature spine

FIGURE 6 Reduced proportion of high-SR ANFs in *Bdnf*^{Pax2} KO mice. (A) Data acquisition was performed by presenting noise-band stimuli in alternating polarity. The round-window recordings of both polarities were averaged in pairs and then bandpass filtered to isolate the neurophonic response. Within a step of rectification, the envelope was calculated and finally averaged for all repetitions. (B) Example trace of a peristimulus time response with a stimulus ranging from 10 to 210 ms during a 400 ms recording window, resulting in a typical slope with a peak and a plateau. (C) The threshold-normalized peak-to-plateau ratio was similar for *Bdnf*^{Pax2} KO mice and controls at 1/3 octave noise bands with a center at 5.7 kHz, (D) 8 kHz, and (E) 11.3 kHz. (F) The peak-to-plateau ratio was reduced in *Bdnf*^{Pax2} KO mice at 16 kHz and at (G) 22.6 kHz. (H) The peak-to-plateau ratio was reduced in *Bdnf*^{Pax2} KO mice when compared for all frequencies at 30 dB above threshold. Mean ± SEM. *$p < .05$, **$p < .01$, ***$p < .001$, ns $p \geq .05$. Detailed statistical information can be found in Table S1.

morphology in the hippocampus of *Bdnf*^{Pax2} KO mice, which otherwise show normal PV-IN numbers, strengthen the assumption that *Bdnf*^{Pax2} KO mice exhibit autism-like structural changes in the HC.

In conclusion, *Bdnf*^{Pax2} KO mice exhibit lower CAP amplitudes and a lower peak-to-plateau ratio of the PSTR predominately in response to higher frequency stimuli. This suggests that high-SR ANF processing did not properly develop in *Bdnf*^{Pax2} KO, possibly due to reduced inhibitory shaping, leading to poor spike synchronization (Graphic Abstract i, controls: left, *Bdnf*^{Pax2} KO: right). Under these conditions, the lack of driving force for tonic inhibition in the ascending pathway would hamper the maturation of inhibitory strength in ascending auditory neurons.[20,21] This prevents proper spike synchronization in *Bdnf*^{Pax2} KO mice, resulting in coarser receptive fields and poorer temporal coding (Graphic Abstract ii). The subsequently elevated spontaneous feed-forward synchronization through the thalamocortical input (Graphic Abstract iii, input MGB) lowers the operation point for signal-to-noise ratio of stimulus-driven pyramidal neurons and stimulus-driven PV-IN inhibition. As a result, enhanced excitability disrupts the internal dynamics of cortical networks, lowering evoked stimulus-driven oscillatory activity and proper network-centered homeostasis for cortical circuit function of coherently activated brain regions (Graphic Abstract iii, output).

5 | DISCUSSION

The cause of altered E/I balance and cortical EEG power changes in autism spectrum disorder, if not hereditary, has remained unclear. Through cortical LFP recordings and their spectral analyses, as well as through CAP and PSTR measurements, to analyze the spike synchronization of ANFs, we discovered that a failed maturation of high-SR ANF processing prevents proper establishment of feed-forward inhibitory networks and homeostasis of intracortical networks after hearing onset, providing a new rationale to explain the development of an autistic phenotype.

5.1 | Reduced evoked and elevated spontaneous local field potentials in *Bdnf*^{Pax2} KO mice

Control mice exhibited a significant increase in LFP amplitude in the AC in response to sound stimuli higher than 6 kHz, which was significantly diminished in *Bdnf*^{Pax2} KO mice (Figure 1). This frequency is within the range in which the hearing of mice is the most sensitive and is considered crucial for communication and behavior.[40,41] Deficits in responses to this frequency range therefore suggest that *Bdnf*^{Pax2} KO mice are severely limited in the processing and integration of behaviorally relevant acoustic information close to threshold. An increased sensitivity to the band of frequencies best for communication gradually developed during evolution to improve communication, mainly through an improved ability to hear higher frequencies.[57,58] While a failure to process sounds in this best frequency range may have only a minimal effect on the survival and evolutionary fitness of non-lingual species such as mice, a similar deficit in humans would have dramatic consequences for behavior, particularly for language acquisition and social learning,[59] notably associated with autism spectrum disorder.[3,17]

A link between autism and deficits in processing sounds in the best frequency range becomes particularly clear when considering the altered cortical LFP response in *Bdnf*^{Pax2} KO mice. Overall and across oscillatory frequency bands, the most profound differences between *Bdnf*^{Pax2} KO mice and controls were seen in response to stimuli higher than 6 kHz. Moreover, *Bdnf*^{Pax2} KO mice exhibited differences in evoked and spontaneous LFP responses in partially overlapping frequency bands in distinct brain regions. These were in part also accompanied by altered induced LFP responses. The reduced evoked LFP responses, higher spontaneous LFP power, and partially elevated induced LFP responses observed in *Bdnf*^{Pax2} KO mice may share a common origin in an elevated ongoing spontaneous activity in the auditory pathway occurring after failed maturation of high-SR ANFs (Graphic Abstract i). This hypothesis is supported through the following observations:

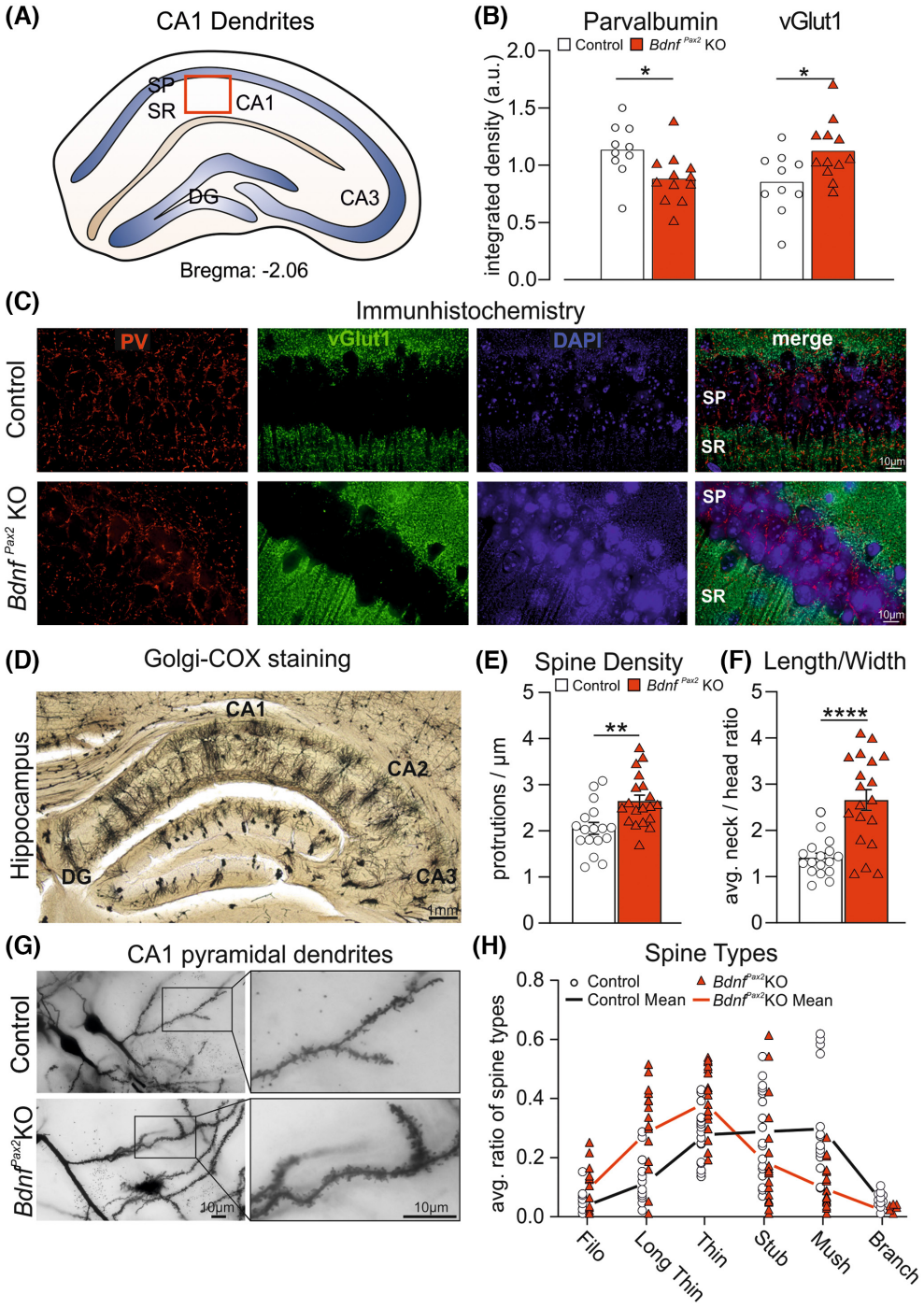

FIGURE 7 Protein analysis of parvalbumin (PV) and vesicular glutamate transporter 1 (vGlut1) and spine analysis in the CA1 region of the hippocampus. (A) Schematic drawing of a coronal section of the hippocampus; DG = dentate gyrus; SP = stratum pyramidale; SR = stratum radiatum. The red box indicates the area analyzed. (B) Quantification of PV and vGlut1 fluorescence in the dendrites of CA1 pyramidal neurons. *Bdnf*^{Pax2} KO mice had lower PV fluorescence intensity and higher vGlut1 fluorescence intensity than controls. (C) Representative images of controls (top) and *Bdnf*^{Pax2}*KO* mice (bottom). (D) Overview picture of the hippocampus after Golgi–Cox staining. (E) Spine analysis of pyramidal neurons in CA1. Spine density is indicated by the number of protrusions per micrometer. Length-to-width ratio (LWR) reflects differences in spine maturation, with higher LWR indicating less mature spines. *Bdnf*^{Pax2} KO mice had significantly higher spine density and LWR than controls, indicating longer, thinner spines (immature spines). (G) Higher magnification of Golgi–Cox-stained CA1 pyramidal neurons of controls (upper panels) and *Bdnf*^{Pax2} KO mice (lower panels). (H) Proportion of different spine types. Control mice had a higher percentage of mature mushroom-type spines and a lower percentage of immature filopodia-type spines than *Bdnf*^{Pax2} KO mice. For C: PV, red; vGlut1, green. DAPI nuclear stain, blue. For B, E, F: *$p < .05$, **$p < .01$, ****$p < .001$. Detailed statistical information can be found in Table S1.

(i) Reduced LFP power in *Bdnf*^{Pax2} KO mice: The elevated spontaneous LFP activity in *Bdnf*^{Pax2} KO mice is comparable to EEG recordings from individuals with Fragile X Syndrome, the leading inherited cause of autism.[60] Recordings in the correspondent *Fmr1* KO mouse also revealed reduced evoked LFPs to sound stimuli along with enhanced induced and spontaneous LFP activity.[60–62]

In *Bdnf*^{Pax2} KO mice, these findings could be linked to an elevated excitatory baseline activity at the thalamocortical input (Graphic Abstract iii). Typically, in a feed-forward mode of function, LFP power in layer IV is defined by thalamocortical input activity, which transmits the input activity of layer IV to infragranular layer V–VI (output) by a large and early current sink into the supragranular layers I-III.[42,63] The layer V–VI output activity influences cognitive top-down modulation, including the PFC and HC.[64–67] The neurons contributing to output activity are extensively shaped by intracortical neural circuits,[68,69] resulting in significantly sharper frequency tuning of neurons that is constructed by output activity rather than input activity.[63] An elevated baseline activity within the ascending auditory pathway that is unable to drive feed-forward inhibition after hearing onset in intracortical (supragranular or infragranular layers) output networks would result in elevated excitatory network responses of output activity. It would thereby provide the explanation for elevated spontaneous LFP power in the AC and coherently activated brain regions in *Bdnf*^{Pax2} KO mice (Figure 3). It would be of interest if individuals suffering from Fragile X Syndrome, or other mouse models for autism spectrum disorder show similar deficits of inhibitory strength along the auditory pathway.

(ii) Reduced ASSRs in *Bdnf*^{Pax2} KO mice: The altered ASSR is perhaps the strongest indicator of an association between the diminished peripheral input of high-SR ANFs and the abnormal intracortical response pattern and autism-like phenotype in *Bdnf*^{Pax2} KO. The ASSR reflects the entrainment of neural activities elicited by periodic auditory stimulation that are sinusoidally modulated in amplitude and frequency. This measurement was used to evaluate sensory and cognitive functions in the central nervous system in numerous clinical studies.[70] Importantly, ASSRs reveal the synchronous discharge of auditory neurons phase-locked to the modulation frequency of the stimulus[71–73] and thereby critically depend on proper phase-locking capacity along the auditory pathway. The power (magnitude) and phase-locking ability (phase consistency across trials) measured with ASSRs is dependent upon the summation of phase-locked activity from multiple neural generators within the auditory system, including the cochlea, auditory nerve, IC, and AC.[43] It is likely that the phase-locked activity of all these neural generators depends on the proper maturation of high-SR ANFs, as this ANF type mainly contributes to the synchronized spike responses within the dynamic range of the auditory nerve response, while low-SR ANFs have limited influence on synchronization.[50] Immaturity of high-SR ANFs would lower synchronization of action potentials to fire sufficiently in phase, as was observed in the profoundly diminished CAP amplitudes in *Bdnf*^{Pax2} KO mice (Figure 5). This would further hamper synchronized spike rates at stimulus onset when the frequency exceeds 11.3 kHz, as observed through the lower PSTR peak-to-plateau ratios in *Bdnf*^{Pax2} KO mice (Figure 6). Moreover, high-SR ANFs are not only predicted to have significant effects on level-dependent response properties[74,75] but they have also been suggested to be primarily responsible for determining ASSR amplitudes at higher SPLs by enabling the activation of frequencies outside of the characteristic frequencies.[44] High-SR ANFs additionally define the perception thresholds at any given characteristic frequency[47,48,51] and thereby, when functionally impaired, would elevate the detection threshold of ASSR signals at low SPLs (Figure 2C,F; Figure S2C,F). Considering this dual function of high-SR ANFs, their impairment in *Bdnf*^{Pax2} KO mice would therefore best explain the severe deficits observed in the ASSR amplitudes in response to stimuli of higher SPLs in the AC and other regions (Figure 2B; Figure S2B,E). The lower evoked and induced ASSRs, observed not only in the AC of *Bdnf*^{Pax2} KO mice but also in the PFC, V1, and HC, may suggest a coherence between these brain regions. Coherence between brain regions activated by amplitude-modulated stimuli has previously been shown for the AC and PFC[76,77] and for the AC and V1.[78,79] This process is driven by feedback from neurons in AC layer V/VI to the dorsal medial geniculate body and the mediodorsal thalamus, which feeds into the PFC and HC.[80,81] In addition, projections from the AC to the V1 have been described.[82]

In analogy, reduced ASSRs and diminished temporal integration and binding of sensory functions across sensory modalities, including multisensory temporal acuity, have been reported in autism spectrum disorder.[3,83,84] These findings support the hypothesis that observed ASSR network changes in the AC and coherent brain regions may be correlates of the autism-like phenotype in *Bdnf*^{Pax2} KO mice.

(iii) Diminished brain oscillations in *Bdnf*^{Pax2} KO mice: Evoked oscillations are stimulus-locked activities and reflect bottom-up sensory transmission by primarily driving inputs.[30,85] Elevated baseline activity, as here hypothesized to occur in *Bdnf*^{Pax2} KO mice, may potentially lower the operation point for stimulus-driven inputs on pyramidal neurons. This imbalance could emerge when tonic inhibition of PV-IN on pyramidal neurons is not properly established during the critical period, as shown previously

in subcortical auditory brainstem regions in *Bdnf*^{Pax2} KO mice.[20] Subsequent to failed maturation of synchronized power to maintain sustained inhibition in the periphery, as here suggested to occur in *Bdnf*^{Pax2} KO mice, cortical pyramidal neurons might be unable to build up sufficient functional surround inhibition and generate sufficient feed-forward synchronization in intracortical networks, which would lead to weaker stimulus-evoked oscillations, as also hypothesized in previous studies.[86,87] In addition, reduced stimulus-evoked intracortical inhibition would further contribute to changes in induced oscillations. Under these conditions, it is thus plausible that the internal dynamics of cortical networks which are critical for establishing and maintaining oscillatory activity and higher cognitive functions[84,88,89] would be impaired in *Bdnf*^{Pax2} KO mice. Fast PV-IN activity in intracortical networks contributes to the generation of oscillatory brain activity during the critical period of sensory experience with slow waves developing earlier than faster ones,[5,9,90–92] explaining the selective effect on EEG power in the alpha and beta bands of *Bdnf*^{Pax2} KO mice. Particular alpha oscillations are suggested to be associated with temporal integration of the different sensory modalities that mature in cascades at different time points, driven by PV-IN networks.[3,5] As in turn the proper integration of all sensory modalities through brain oscillation, driven by PV-IN networks, is a prerequisite for attentional control of speech processing and verbal fluency in humans,[7] diminished alpha band oscillations in *Bdnf*^{Pax2} KO mice would be one of the most critical links to their cognitive deficits. In line with these observations, reduced evoked brain activity across alpha, beta, and low-gamma oscillations is a characteristic feature of the early-onset "critical period" disorders, such as autism,[3–7] as opposed to late-onset psychiatric disorders, such as schizophrenia, which are characterized primarily by reduced evoked gamma oscillations.[93]

Until now, the source of enhanced spontaneous and reduced evoked broadband EEG power in autism, if not hereditary, has remained unknown. The time period in which autism symptoms start to manifest (three to six months of age) is the same period in which children exhibit a dramatic shift in their EEG power spectrum, resulting from changes in conduction speed, synapse number and strength, and cellular composition and maturity.[5] During this time, EEG waveforms are assumed to integrate neuronal activity driven by the individual sensory modalities.[9,90] It has long been hypothesized that if sensory input was integrated improperly in higher brain regions regarding its modality, it would result in deficits in complex executive behavior, such as language in autism.[3] While improper sensory integration could occur because of sensory deprivation, autism spectrum disorder in children is typically associated with normal basic sensory function,[17,59,94] which would exclude sensory deprivation as a main cause of altered cortical brain oscillations.

These data provide a new understanding of autism through an immature synchronization of peripheral neuronal processes. This peripheral immaturity would, despite the development of basic hearing function, prevent the maturation of intracortical networks that allow the processing of higher frequencies critical for communication.

(iv) E/I imbalance in *Bdnf*^{Pax2} KO mice: Numerous studies in both humans[4,95] and animals[89] emphasize E/I imbalance in frontal brain regions as a characteristic feature of autism. E/I imbalance has been suggested to involve aberrant neural connectivity linked to a reduction of brain volume in the frontal cortex and HC linked with a loss of synapses rather than neurons themselves.[96,97] Indeed, psychiatric disorders have been associated with reduced dendritic outgrowths of PV-INs and with more immature dendritic spines on pyramidal cells in postmortem studies[96,97] and in mouse models.[98] In line with this, *Bdnf*^{Pax2} KO mice exhibit normal numbers of PV-INs and normal BDNF mRNA/protein levels in the AC and HC, but immature (low) levels of PV in dendrites that persist also into adulthood (Figure S4).[20,21] As shown in the present study, *Bdnf*^{Pax2} KO mice exhibit reduced PV-IN staining and enhanced vGlut1 levels in hippocampal stratum radiatum (Figure 7), confirming E/I imbalance to occur on synaptic levels.

The normal PV-IN number in the cortex of *Bdnf*^{Pax2} KO mice suggests that the source of the structural and functional E/I imbalance in the cortex and HC of *Bdnf*^{Pax2} KO mice is neither a general impairment in the migration of GABAergic INs from the subpallium to telencephalon[14,27] nor a lack of cortical BDNF in pyramidal neurons, required for the experience-driven synaptogenesis of fast-spiking PV-INs and pyramidal neurons.[22,23,99]

The Pax2+ GABAergic IN precursor cells, suggested to be impaired in *Bdnf*^{Pax2} KO mice, derive from the third ventricle and migrate to hindbrain regions and the auditory periphery, including ANFs.[27,29] It was previously shown that BDNF deletion in Pax2-lineage descendants resulted in reduced sustained tonic inhibitory strength of the high-frequency sidebands of sharply tuned projecting neurons in the DCN and IC, particularly in response to stimuli with frequencies higher than 10 kHz.[20,21,33] The fact that *Bdnf*^{Pax2} KO mice exhibit deficits in higher frequency responses in (i) CAP amplitudes and PSTR peak-to-plateau ratios (Figures 5 and 6), (ii) high-frequency sideband inhibition in the DCN and IC,[20,21] and (iii) cortical LFP responses (Figure 1; Figure 4) underscores a relationship between these processes.

We hypothesize that the mechanism behind the influence of BDNF deletion in Pax2-lineage descendants

on high-SR fiber processing is an impaired maturation of inhibitory lateral olivocochlear (LOC) efferents. LOC efferents modulate high-SR ANF responses through axo-dendritic tonic inhibition. When this inhibition is impaired, spontaneous firing rates of ANFs are elevated, while response amplitudes of particularly high-SR ANFs are reduced.[100] Hypothesizing that in *Bdnf*^{Pax2} KO mice, the shaping of auditory nerve responses remains immature, we would expect a reduced activation of dendrites contacting DCN neurons, leading to longer membrane time constraints that would consequently widen the temporal window for specific high-frequency sensory-evoked information.[101] This accounts for the observed elevated thresholds, enlarged bandwidth, and reduced high-frequency sideband inhibition accompanied by elevated firing rates observed in the DCN[20] and IC of *Bdnf*^{Pax2} KO mice.[21] Dysfunctional inhibitory shaping of ANFs following impaired function of Pax2+ precursor cells—as postulated here—may also provide the connection to reduced GABA function in autism: During the critical period—the suspected onset of autism[4,5,18]—GABA receptor function switches from excitatory to inhibitory in all sensory systems.[102,103] During this time, an upregulation of the potassium chloride cotransporter 2 (KCC2) in INs, strongly modulated by activity-driven BDNF, is suggested to promote the excitatory-to-inhibitory switch in GABAergic signaling in a region- and modality-specific manner.[104–107] High-SR ANFs were previously suggested to drive this switch through activity-driven BDNF upregulation.[45,108] In support of this proposed mechanism, auditory nerve transection that includes high-SR ANFs leads to a decline of KCC2 and a subsequent re-emergence of depolarizing GABAergic signaling.[109] Furthermore, a deafferentation of ANFs after acoustic trauma that, from its percentage, includes high-SR ANFs triggers a reduction of activity-driven BDNF expression levels in the auditory brainstem.[34] An imbalance of excitatory/inhibitory effects of GABA would also explain elevated epileptiform activity observed in children with autism spectrum disorders and reduced GABAergic activity in the brain in humans[4,95] and mouse models.[15]

In conclusion, diminished high-SR ANF processing in *Bdnf*^{Pax2} KO mice would primarily influence synchronized spike responses,[110] evoked population synchrony,[38,50] and diminished tonic inhibition in ascending circuits, thereby diminishing the network-centered homeostasis of the overall cortical circuit and ultimately resulting in an autistic phenotype. This is expected to affect the corticofugal feedback loops which, as postulated by others,[64,111,112] control perception and attention. Based on the current findings, these should be reconsidered in the context of the influence of LOC activation o high-SR ANFs as also postulated previously.[111]

In the light of this new perspective, various observations made in the context of autism require further examination: (i) Disturbed feed-forward and intracortical synchronization, as observed in *Bdnf*^{Pax2} KO mice,[45] may provide a rationale for predictive coding deficits observed in autism spectrum disorder.[113,114] (ii) Deficits in the visual orientation tuning of the autistic *Fmr1* KO mice model linked to decreased PV-IN activity in V1[19] can be considered within the context of a thus far unknown source in the retina that may provide improved driving force for central inhibition in the visual cortex. This may also be reconsidered in the context of the reduction of cortical signal power at alpha and beta frequencies in the visual system of autistic human subjects, discussed in the context of impaired cortico-cortical feedback for contextual cues.[114,115] (iii) In the context of the present findings, deficits in high-SR ANF function can be reconsidered as a source of immediate unmasking of cortical neurons after peripheral damage without causing a change in topographic map plasticity.[87] Through such an event, the increased risk for cognitive deficits observed with hearing loss[116,117] or listening difficulties in children with clinically normal hearing[17,59,118–121] may be explained. (iv) Any processes of either hereditary or acquired origin that might disrupt proper migration of GABA-IN precursor neurons to brainstem regions, including intraventricular or periventricular hemorrhage, or hypoxic ischemic encephalopathies, linked with neonatal bleeding during the critical developmental period of children,[122] should be newly reconsidered as a possible cause of autism.

5.2 | Limitations of the study

Though it is important to acknowledge that neuro-oscillatory frequency bands in rodents may not directly correspond to those in the primate brain,[85] there is meanwhile evidence that brain oscillations, including slower ones, can indicate compatible neural processes in different species, including rodents.[10]

A clear connection between the role of high-SR processing, KCC2, and BDNF has not been brought and likely cannot be provided due to the enormous complexity of the integrated networks, which exhibit modality-specificity and high variability in temporal and spatial dynamics due to the cascading development of sensory modalities during critical developmental periods.[5,102,103] This includes the predicted need of proper tonic GABAergic activity for spine maturation that cannot be proven beyond doubt due to temporal and spatial heterogeneity of circuits involved.[123] The relationship between lower inhibitory GABAergic processing in *Bdnf*^{Pax2} KO mice and an

observed immature pattern of spine density in *Bdnf*^{Pax2} KO (Figure 7), both described in autism,[96,97,124] cannot be established causally for the same reason.

In addition, the migration of Pax2-positive GABAergic precursor neurons and the function of BDNF for this process are not generally very well studied or understood and require more in-depth investigations.

AUTHOR CONTRIBUTIONS

Designed research: Marlies Knipper, Philine Marchetta, and Lukas Rüttiger. Performed research: Philine Marchetta, Morgan Hess, Dila Calis, Rüdiger Land, Stefan Fink, and Kerstin Schwabe. Contributed unpublished reagents/analytic tools: Jean-Luc Puel, Jerome Bourien, Konrad Dapper, Michele H. Jacob, Mesbah Alam, and Kerstin Schwabe. Analyzed data: Philine Marchetta, Konrad Dapper, Morgan Hess, Dila Calis, Wibke Singer, Jakob Wertz, Stefan Fink, Matthias H. J. Munk, and Rüdiger Land. Wrote the paper: Marlies Knipper, Rüdiger Land, Matthias H. J. Munk, Philine Marchetta, Morgan Hess, Konrad Dapper, and Lukas Rüttiger. Edited the paper: Morgan Hess, Matthias H. J. Munk, Lukas Rüttiger, Rüdiger Land, Konrad Dapper, Marlies Knipper, Michele H. Jacob, Konrad Dapper, and Robert Lukowski.

ACKNOWLEDGMENTS

We thank Hyun-Soon Geisler and Karin Rohbock for excellent technical assistance. Open Access funding enabled and organized by Projekt DEAL.

FUNDING INFORMATION

DFG; FOR 2060 project RU 713/3-2 (MK, LR, and WS). DFG; FOR 2060 project KN 316/12-1 (MK and MH). DFG; GRK 2381 (PM, DC, RLu, and MJ). ERA-NET NEURON JTC 2020: BMBF 01EW2102 CoSySpeech FWO G0H6420N (JB, JLB, KD, and MM). DFG; Cluster of Excellence 2177 "Hearing4all" Project number 390895286 (RLa, KS, and MA).

DISCLOSURES

The authors declare that they have no competing interests.

DATA AVAILABILITY STATEMENT

All data needed to evaluate the conclusions in the paper are present in the paper and/or the Supplementary Materials. All data can be provided by the authors, and requests should be submitted to the corresponding author.

ORCID

Philine Marchetta https://orcid.org/0000-0003-0685-2805
Konrad Dapper https://orcid.org/0009-0007-7385-8031
Morgan Hess https://orcid.org/0009-0009-0713-9834
Wibke Singer https://orcid.org/0000-0002-2242-7174
Stefan Fink https://orcid.org/0000-0002-7938-9869
Steffen R. Hage https://orcid.org/0000-0002-7018-543X
Mesbah Alam https://orcid.org/0009-0009-8140-1933
Kerstin Schwabe https://orcid.org/0000-0002-2041-066X
Robert Lukowski https://orcid.org/0000-0002-4564-3574
Jerome Bourien https://orcid.org/0000-0001-5860-5772
Jean-Luc Puel https://orcid.org/0000-0002-3772-5190
Michele H. Jacob https://orcid.org/0000-0002-7008-839X
Matthias H. J. Munk https://orcid.org/0000-0002-5339-4045
Rüdiger Land https://orcid.org/0000-0003-0264-585X
Lukas Rüttiger https://orcid.org/0000-0003-0015-0714
Marlies Knipper https://orcid.org/0000-0002-6181-5735

REFERENCES

1. Lord C, Elsabbagh M, Baird G, Veenstra-Vanderweele J. Autism spectrum disorder. *Lancet*. 2018;392:508-520.
2. Vorstman JAS, Parr JR, Moreno-De-Luca D, Anney RJL, Nurnberger JI Jr, Hallmayer JF. Autism genetics: opportunities and challenges for clinical translation. *Nat Rev Genet*. 2017;18:362-376.
3. LeBlanc, J. J., and Fagiolini, M. (2011) Autism: a "critical period" disorder? *Neural Plast* 2011, 921680.
4. Ben-Ari Y. Is birth a critical period in the pathogenesis of autism spectrum disorders? *Nat Rev Neurosci*. 2015;16:498-505.
5. Reh RK, Dias BG, Nelson CA 3rd, et al. Critical period regulation across multiple timescales. *Proc Natl Acad Sci U S A*. 2020;117:23242-23251.
6. Gabard-Durnam LJ, Wilkinson C, Kapur K, Tager-Flusberg H, Levin AR, Nelson CA. Longitudinal EEG power in the first postnatal year differentiates autism outcomes. *Nat Commun*. 2019;10:4188.
7. Levin AR, Varcin KJ, O'Leary HM, Tager-Flusberg H, Nelson CA. EEG power at 3 months in infants at high familial risk for autism. *J Neurodev Disord*. 2017;9:34.
8. Hu H, Gan J, Jonas P. Interneurons. Fast-spiking, parvalbumin^{+} GABAergic interneurons: from cellular design to microcircuit function. *Science*. 2014;345:1255263.
9. Bartos M, Vida I, Jonas P. Synaptic mechanisms of synchronized gamma oscillations in inhibitory interneuron networks. *Nat Rev Neurosci*. 2007;8:45-56.
10. Chen G, Zhang Y, Li X, et al. Distinct inhibitory circuits orchestrate cortical beta and gamma band oscillations. *Neuron*. 2017;96:1403-1418.e1406.
11. Galuske RAW, Munk MHJ, Singer W. Relation between gamma oscillations and neuronal plasticity in the visual cortex. *Proc Natl Acad Sci U S A*. 2019;116:23317-23325.
12. Levin AR, Nelson CA. Inhibition-based biomarkers for autism spectrum disorder. *Neurotherapeutics*. 2015;12:546-552.
13. Southwell DG, Nicholas CR, Basbaum AI, et al. Interneurons from embryonic development to cell-based therapy. *Science*. 2014;344:1240622.
14. Marin O. Interneuron dysfunction in psychiatric disorders. *Nat Rev Neurosci*. 2012;13:107-120.

15. Gogolla N, LeBlanc JJ, Quast KB, Südhof TC, Fagiolini M, Hensch TK. Common circuit defect of excitatory-inhibitory balance in mouse models of autism. *J Neurodev Disord*. 2009;1:172-181.
16. Bartolini G, Ciceri G, Marín O. Integration of GABAergic interneurons into cortical cell assemblies: lessons from embryos and adults. *Neuron*. 2013;79:849-864.
17. Foss-Feig JH, Schauder KB, Key AP, Wallace MT, Stone WL. Audition-specific temporal processing deficits associated with language function in children with autism spectrum disorder. *Autism Res*. 2017;10:1845-1856.
18. Werker JF, Hensch TK. Critical periods in speech perception: new directions. *Annu Rev Psychol*. 2015;66:173-196.
19. Goel A, Cantu DA, Guilfoyle J, et al. Impaired perceptual learning in a mouse model of fragile X syndrome is mediated by parvalbumin neuron dysfunction and is reversible. *Nat Neurosci*. 2018;21:1404-1411.
20. Eckert P, Marchetta P, Manthey MK, et al. Deletion of BDNF in Pax2 lineage-derived interneuron precursors in the hindbrain hampers the proportion of excitation/inhibition, learning, and behavior. *Front Mol Neurosci*. 2021;14:642679.
21. Chumak T, Rüttiger L, Lee SC, et al. BDNF in lower brain parts modifies auditory fiber activity to gain Fidelity but increases the risk for generation of central noise after injury. *Mol Neurobiol*. 2016;53:5607-5627.
22. Xu H, Kotak VC, Sanes DH. Normal hearing is required for the emergence of long-lasting inhibitory potentiation in cortex. *J Neurosci*. 2010;30:331-341.
23. Lehmann K, Steinecke A, Bolz J. GABA through the ages: regulation of cortical function and plasticity by inhibitory interneurons. *Neural Plast*. 2012;2012:892784.
24. Lewis DA. Inhibitory neurons in human cortical circuits: substrate for cognitive dysfunction in schizophrenia. *Curr Opin Neurobiol*. 2014;26:22-26.
25. Lech MA, Leśkiewicz M, Kamińska K, Rogóż Z, Lorenc-Koci E. Glutathione deficiency during early postnatal development causes schizophrenia-like symptoms and a reduction in BDNF levels in the cortex and hippocampus of adult Sprague–Dawley rats. *Int J Mol Sci*. 2021;22:6171.
26. Guo J, Anton ES. Decision making during interneuron migration in the developing cerebral cortex. *Trends Cell Biol*. 2014;24:342-351.
27. Maricich SM, Herrup K. Pax-2 expression defines a subset of GABAergic interneurons and their precursors in the developing murine cerebellum. *J Neurobiol*. 1999;41:281-294.
28. Larsson M. Pax2 is persistently expressed by GABAergic neurons throughout the adult rat dorsal horn. *Neurosci Lett*. 2017;638:96-101.
29. Rowitch DH, Kispert A, McMahon AP. Pax-2 regulatory sequences that direct transgene expression in the developing neural plate and external granule cell layer of the cerebellum. *Brain Res Dev Brain Res*. 1999;117:99-108.
30. David O, Kilner JM, Friston KJ. Mechanisms of evoked and induced responses in MEG/EEG. *Neuroimage*. 2006;31:1580-1591.
31. Ohyama T, Groves AK. Generation of Pax2-Cre mice by modification of a Pax2 bacterial artificial chromosome. *Genesis*. 2004;38:195-199.
32. Rios M, Fan G, Fekete C, et al. Conditional deletion of brain-derived neurotrophic factor in the postnatal brain leads to obesity and hyperactivity. *Mol Endocrinol*. 2001;15:1748-1757.
33. Zuccotti A, Kuhn S, Johnson SL, et al. Lack of brain-derived neurotrophic factor hampers inner hair cell synapse physiology, but protects against noise-induced hearing loss. *J Neurosci*. 2012;32:8545-8553.
34. Matt L, Eckert P, Panford-Walsh R, et al. Visualizing BDNF transcript usage during sound-induced memory linked plasticity. *Front Mol Neurosci*. 2018;11:260.
35. Singer W, Geisler HS, Panford-Walsh R, Knipper M. Detection of excitatory and inhibitory synapses in the auditory system using fluorescence immunohistochemistry and high-resolution fluorescence microscopy. *Methods Mol Biol*. 2016;1427:263-276.
36. Franklin KBJ, Paxinos G. *The Mouse Brain in Stereotaxic Coordinates*. Vol 3. Academic Press; 2008.
37. Singer W, Geisler HS, Knipper M. The Geisler method: tracing activity-dependent cGMP plasticity changes upon double detection of mRNA and protein on brain slices. *Methods Mol Biol*. 2013;1020:223-233.
38. Huet A, Batrel C, Dubernard X, et al. Peristimulus time responses predict adaptation and spontaneous firing of auditory-nerve fibers: from rodents data to humans. *J Neurosci*. 2022;42:2253-2267.
39. Risher WC, Ustunkaya T, Singh Alvarado J, Eroglu C. Rapid Golgi analysis method for efficient and unbiased classification of dendritic spines. *PloS One*. 2014;9:e107591.
40. Hage SR, Ehret G. Mapping responses to frequency sweeps and tones in the inferior colliculus of house mice. *Eur J Neurosci*. 2003;18:2301-2312.
41. Hernández O, Espinosa N, Pérez-González D, Malmierca M. The inferior colliculus of the rat: a quantitative analysis of monaural frequency response areas. *Neuroscience*. 2005;132:203-217.
42. Einevoll GT, Kayser C, Logothetis NK, Panzeri S. Modelling and analysis of local field potentials for studying the function of cortical circuits. *Nat Rev Neurosci*. 2013;14:770-785.
43. Lu H, Mehta AH, Oxenham AJ. Methodological considerations when measuring and analyzing auditory steady-state responses with multi-channel EEG. *Curr Res Neurobiol*. 2022;3:100061.
44. Encina-Llamas G, Harte JM, Dau T, Shinn-Cunningham B, Epp B. Investigating the effect of cochlear synaptopathy on envelope following responses using a model of the auditory nerve. *J Assoc Res Otolaryngol*. 2019;20:363-382.
45. Knipper M, Singer W, Schwabe K, et al. Disturbed balance of inhibitory signaling links hearing loss and cognition. *Front Neural Circuits*. 2022;15:785603.
46. Bharadwaj HM, Masud S, Mehraei G, Verhulst S, Shinn-Cunningham BG. Individual differences reveal correlates of hidden hearing deficits. *J Neurosci*. 2015;35:2161-2172.
47. Meddis R. Auditory-nerve first-spike latency and auditory absolute threshold: a computer model. *J Acoust Soc Am*. 2006;119:406-417.
48. Heil P, Neubauer H, Brown M, Irvine DR. Towards a unifying basis of auditory thresholds: distributions of the first-spike latencies of auditory-nerve fibers. *Hear Res*. 2008;238:25-38.
49. Liberman MC, Dodds LW. Single-neuron labeling and chronic cochlear pathology. III. Stereocilia damage and alterations of threshold tuning curves. *Hear Res*. 1984;16:55-74.
50. Huet A, Batrel C, Wang J, et al. Sound coding in the auditory nerve: from single fiber activity to Cochlear mass potentials in gerbils. *Neuroscience*. 2019;407:83-92.

51. Bourien J, Tang Y, Batrel C, et al. Contribution of auditory nerve fibers to compound action potential of the auditory nerve. *J Neurophysiol*. 2014;112:1025-1039.
52. Batrel C, Huet A, Hasselmann F, et al. Mass potentials recorded at the round window enable the detection of low spontaneous rate fibers in gerbil auditory nerve. *PLoS ONE*. 2017;12:e0169890.
53. Hutsler JJ, Zhang H. Increased dendritic spine densities on cortical projection neurons in autism spectrum disorders. *Brain Res*. 2010;1309:83-94.
54. Li B-Z, Sumera A, Booker SA, McCullagh EA. Current best practices for analysis of dendritic spine morphology and number in neurodevelopmental disorder research. *ACS Chem Nerosci*. 2023;14:1561-1572.
55. Schmeisser MJ, Ey E, Wegener S, et al. Autistic-like behaviours and hyperactivity in mice lacking ProSAP1/Shank2. *Nature*. 2012;486:256-260.
56. Strackeljan L, Baczynska E, Cangalaya C, et al. Microglia depletion-induced remodeling of extracellular matrix and excitatory synapses in the hippocampus of adult mice. *Cell*. 2021;10:1862.
57. Manley GA. Some aspects of the evolution of hearing in vertebrates. *Nature*. 1971;230:506-509.
58. Fisch L. Integrated development and maturation of the hearing system. A critical review article. *Br J Audiol*. 1983;17:137-154.
59. Fitch RH, Alexander ML, Threlkeld SW. Early neural disruption and auditory processing outcomes in rodent models: implications for developmental language disability. *Front Syst Neurosci*. 2013;7:58.
60. Holley AJ, Shedd A, Boggs A, et al. A sound-driven cortical phase-locking change in the Fmr1 KO mouse requires Fmr1 deletion in a subpopulation of brainstem neurons. *Neurobiol Dis*. 2022;170:105767.
61. Ethridge LE, White SP, Mosconi MW, et al. Neural synchronization deficits linked to cortical hyper-excitability and auditory hypersensitivity in fragile X syndrome. *Mol Autism*. 2017;8:1-11.
62. Jonak CR, Lovelace JW, Ethell IM, Razak KA, Binder DK. Multielectrode array analysis of EEG biomarkers in a mouse model of fragile X syndrome. *Neurobiol Dis*. 2020;138:104794.
63. Liu X, Zhou L, Ding F, Wang Y, Yan J. Local field potentials are local events in the mouse auditory cortex. *Eur J Neurosci*. 2015;42:2289-2297.
64. Antunes FM, Malmierca MS. Corticothalamic pathways in auditory processing: recent advances and insights from other sensory systems. *Frontiers in Neural Circuits*. 2021;15:721186.
65. Asilador A, Llano DA. Top-down inference in the auditory system: potential roles for Corticofugal projections. *Frontiers in Neural Circuits*. 2021;14:615259.
66. Tabas A, von Kriegstein K. Adjudicating between local and global architectures of predictive processing in the subcortical auditory pathway. *Front Neural Circuits*. 2021;15:644743.
67. Terreros G, Delano PH. Corticofugal modulation of peripheral auditory responses. *Front Syst Neurosci*. 2015;9:134.
68. Eggermont JJ, Munguia R, Pienkowski M, Shaw G. Comparison of LFP-based and spike-based spectro-temporal receptive fields and cross-correlation in cat primary auditory cortex. *PloS One*. 2011;6:e20046.
69. de Cheveigne A, Edeline JM, Gaucher Q, Gourevitch B. Component analysis reveals sharp tuning of the local field potential in the Guinea pig auditory cortex. *J Neurophysiol*. 2013;109:261-272.
70. Parker EM, Sweet RA. Stereological assessments of neuronal pathology in auditory cortex in schizophrenia. *Front Neuroanat*. 2017;11:131.
71. Brenner CA, Krishnan GP, Vohs JL, et al. Steady state responses: electrophysiological assessment of sensory function in schizophrenia. *Schizophr Bull*. 2009;35:1065-1077.
72. Kuwada S, Anderson JS, Batra R, Fitzpatrick DC, Teissier N, D'Angelo WR. Sources of the scalp-recorded amplitude-modulation following response. *J Am Acad Audiol*. 2002;13:188-204.
73. Parthasarathy A, Bartlett E. Two-channel recording of auditory-evoked potentials to detect age-related deficits in temporal processing. *Hear Res*. 2012;289:52-62.
74. Liberman MC, Kiang NY. Single-neuron labeling and chronic cochlear pathology. IV. Stereocilia damage and alterations in rate- and phase-level functions. *Hear Res*. 1984;16:75-90.
75. Marcher-Rorsted J, Encina-Llamas G, Dau T, Liberman MC, Wu PZ, Hjortkjaer J. Age-related reduction in frequency-following responses as a potential marker of cochlear neural degeneration. *Hear Res*. 2022;414:108411.
76. Wang Y, Li Z, Tian Z, Wang X, Li Y, Qin L. Emotional arousal modifies auditory steady state response in the auditory cortex and prefrontal cortex of rats. *Stress*. 2019;22:492-500.
77. Wieczerzak KB, Patel SV, MacNeil H, et al. Differential plasticity in auditory and prefrontal cortices, and cognitive-behavioral deficits following noise-induced hearing loss. *Neuroscience*. 2021;455:1-18.
78. Schormans AL, Typlt M, Allman BL. Crossmodal plasticity in auditory, visual and multisensory cortical areas following noise-induced hearing loss in adulthood. *Hear Res*. 2017;343:92-107.
79. Drijvers L, Jensen O, Spaak E. Rapid invisible frequency tagging reveals nonlinear integration of auditory and visual information. *Hum Brain Mapp*. 2021;42:1138-1152.
80. Mease RA, Gonzalez AJ. Corticothalamic pathways from layer 5: emerging roles in computation and pathology. *Front Neural Circuits*. 2021;15:730211.
81. Bueno-Junior LS, Leite JP. Input convergence, synaptic plasticity and functional coupling across hippocampal-prefrontal-thalamic circuits. *Front Neural Circuits*. 2018;12:40.
82. Hall AJ, Lomber SG. Auditory cortex projections target the peripheral field representation of primary visual cortex. *Exp Brain Res*. 2008;190:413-430.
83. Hirano Y, Oribe N, Kanba S, Onitsuka T, Nestor PG, Spencer KM. Spontaneous gamma activity in schizophrenia. *JAMA Psychiatry*. 2015;72:813-821.
84. Hirano Y, Nakamura I, Tamura S, Onitsuka T. Long-term test-retest reliability of auditory gamma oscillations between different clinical EEG systems. *Front Psych*. 2020;11:876.
85. Buzsaki G, Logothetis N, Singer W. Scaling brain size, keeping timing: evolutionary preservation of brain rhythms. *Neuron*. 2013;80:751-764.
86. Calford MB, Tweedale R. C-fibres provide a source of masking inhibition to primary somatosensory cortex. *Proc Roy Soc London Ser B Biol Sci*. 1991;243:269-275.

87. Rajan R. Receptor organ damage causes loss of cortical surround inhibition without topographic map plasticity. *Nat Neurosci*. 1998;1:138-143.
88. Uhlhaas PJ, Singer W. Abnormal neural oscillations and synchrony in schizophrenia. *Nat Rev Neurosci*. 2010;11:100-113.
89. Onitsuka T, Tsuchimoto R, Oribe N, Spencer KM, Hirano Y. Neuronal imbalance of excitation and inhibition in schizophrenia: a scoping review of gamma-band ASSR findings. *Psychiatry Clin Neurosci*. 2022;76:610-619.
90. Sohal VS, Zhang F, Yizhar O, Deisseroth K. Parvalbumin neurons and gamma rhythms enhance cortical circuit performance. *Nature*. 2009;459:698-702.
91. Miyamoto H, Katagiri H, Hensch T. Experience-dependent slow-wave sleep development. *Nat Neurosci*. 2003;6:553-554.
92. Chen G, Rasch MJ, Wang R, Zhang XH. Experience-dependent emergence of beta and gamma band oscillations in the primary visual cortex during the critical period. *Sci Rep*. 2015;5:17847.
93. Hunt MJ, Kopell NJ, Traub RD, Whittington MA. Aberrant network activity in schizophrenia. *Trends Neurosci*. 2017;40:371-382.
94. Mamashli F, Khan S, Bharadwaj H, et al. Auditory processing in noise is associated with complex patterns of disrupted functional connectivity in autism spectrum disorder. *Autism Res*. 2017;10:631-647.
95. Port RG, Gaetz W, Bloy L, et al. Exploring the relationship between cortical GABA concentrations, auditory gamma-band responses and development in ASD: evidence for an altered maturational trajectory in ASD. *Autism Res*. 2017;10:593-607.
96. Glantz LA, Lewis DA. Decreased dendritic spine density on prefrontal cortical pyramidal neurons in schizophrenia. *Arch Gen Psychiatry*. 2000;57:65-73.
97. Osimo EF, Beck K, Reis Marques T, Howes OD. Synaptic loss in schizophrenia: a meta-analysis and systematic review of synaptic protein and mRNA measures. *Mol Psychiatry*. 2019;24:549-561.
98. Kolomeets NS, Orlovskaya DD, Uranova NA. Decreased numerical density of CA3 hippocampal mossy fiber synapses in schizophrenia. *Synapse*. 2007;61:615-621.
99. Kimura F, Itami C. A hypothetical model concerning how spike-timing-dependent plasticity contributes to neural circuit formation and initiation of the critical period in barrel cortex. *J Neurosci*. 2019;39:3784-3791.
100. Ruel J, Nouvian R, Gervais d'Aldin C, Pujol R, Eybalin M, Puel JL. Dopamine inhibition of auditory nerve activity in the adult mammalian cochlea. *Eur J Neurosci*. 2001;14:977-986.
101. Kopp-Scheinpflug C, Tozer AJ, Robinson SW, Tempel BL, Hennig MH, Forsythe ID. The sound of silence: ionic mechanisms encoding sound termination. *Neuron*. 2011;71:911-925.
102. Kandler K, Friauf E. Development of glycinergic and glutamatergic synaptic transmission in the auditory brainstem of perinatal rats. *J Neurosci*. 1995;15:6890-6904.
103. Friauf E, Rust MB, Schulenborg T, Hirtz JJ. Chloride cotransporters, chloride homeostasis, and synaptic inhibition in the developing auditory system. *Hear Res*. 2011;279:96-110.
104. Wardle RA, Poo MM. Brain-derived neurotrophic factor modulation of GABAergic synapses by postsynaptic regulation of chloride transport. *J Neurosci*. 2003;23:8722-8732.
105. Rivera C, Voipio J, Kaila K. Two developmental switches in GABAergic signalling: the K+-Cl- cotransporter KCC2 and carbonic anhydrase CAVII. *J Physiol*. 2005;562:27-36.
106. Gagnon M, Bergeron MJ, Lavertu G, et al. Chloride extrusion enhancers as novel therapeutics for neurological diseases. *Nat Med*. 2013;19:1524-1528.
107. Kaila K, Price TJ, Payne JA, Puskarjov M, Voipio J. Cation-chloride cotransporters in neuronal development, plasticity and disease. *Nat Rev Neurosci*. 2014;15:637-654.
108. Knipper M, van Dijk P, Schulze H, et al. The neural bases of tinnitus: lessons from deafness and Cochlear implants. *J Neurosci*. 2020;40:7190-7202.
109. Tighilet B, Dutheil S, Siponen MI, Norena AJ. Reactive neurogenesis and Down-regulation of the potassium-chloride cotransporter KCC2 in the Cochlear nuclei after Cochlear deafferentation. *Front Pharmacol*. 2016;7:281.
110. Buran BN, Strenzke N, Neef A, Gundelfinger ED, Moser T, Liberman MC. Onset coding is degraded in auditory nerve fibers from mutant mice lacking synaptic ribbons. *J Neurosci*. 2010;30:7587-7597.
111. Lauer AM, Jimenez SV, Delano PH. Olivocochlear efferent effects on perception and behavior. *Hear Res*. 2022;419:108207.
112. Elgueda D, Ayala YA, Delano PH. Editorial: listening in action: attention, emotions and cognition in the auditory system. *Front Neurosci*. 2022;16:1007095.
113. Idei H, Murata S, Yamashita Y, Ogata T. Homogeneous intrinsic neuronal excitability induces overfitting to sensory noise: a robot model of neurodevelopmental disorder. *Front Psych*. 2020;11:762.
114. Brodski-Guerniero A, Naumer MJ, Moliadze V, et al. Predictable information in neural signals during resting state is reduced in autism spectrum disorder. *Hum Brain Mapp*. 2018;39:3227-3240.
115. Seymour RA, Rippon G, Gooding-Williams G, Schoffelen JM, Kessler K. Dysregulated oscillatory connectivity in the visual system in autism spectrum disorder. *Brain*. 2019;142:3294-3305.
116. Livingston G, Sommerlad A, Orgeta V, et al. Dementia prevention, intervention, and care. *Lancet*. 2017;390:2673-2734.
117. Griffiths TD, Lad M, Kumar S, et al. How can hearing loss cause dementia? *Neuron*. 2020;108:401-412.
118. Moore DR, Sieswerda SL, Grainger MM, et al. Referral and diagnosis of developmental auditory processing disorder in a large, United States hospital-based audiology service. *J Am Acad Audiol*. 2018;29:364-377.
119. Stewart HJ, Cash EK, Pinkl J, et al. Adaptive hearing aid benefit in children with mild/moderate hearing loss: a registered, double-blind, randomized clinical trial. *Ear Hear*. 2022;43:1402-1415.
120. Moore DR, Zobay O, Ferguson MA. Minimal and mild hearing loss in children: association with auditory perception, cognition, and communication problems. *Ear Hear*. 2020;41:720-732.
121. Petley L, Hunter LL, Motlagh Zadeh L, et al. Listening difficulties in children with Normal audiograms: relation to hearing and cognition. *Ear Hear*. 2021;42:1640-1655.
122. Volpe JJ. Brain injury in premature infants: a complex amalgam of destructive and developmental disturbances. *Lancet Neurol*. 2009;8:110-124.

123. Awad PN, Amegandjin CA, Szczurkowska J, et al. KCC2 regulates dendritic spine formation in a brain-region specific and BDNF dependent manner. *Cereb Cortex*. 2018;28:4049-4062.
124. Alexander JM, Pirone A, Jacob MH. Excessive beta-catenin in excitatory neurons results in reduced social and increased repetitive behaviors and altered expression of multiple genes linked to human autism. *Front Synaptic Neurosci*. 2020;12:14.

SUPPORTING INFORMATION

Additional supporting information can be found online in the Supporting Information section at the end of this article.

How to cite this article: Marchetta P, Dapper K, Hess M, et al. Dysfunction of specific auditory fibers impacts cortical oscillations, driving an autism phenotype despite near-normal hearing. *The FASEB Journal*. 2024;38:e23411. doi:10.1096/fj.202301995R